Quarterly Progress Report

N01-NS-1-2333

Restoration of Hand and Arm Function by Functional Neuromuscular Stimulation

Period covered: April 1, 2003 to June 30, 2003

Principal Investigator: Robert F. Kirsch, Ph.D.

Co-Investigators:

Patrick E. Crago, Ph.D.
P. Hunter Peckham, Ph.D.
Warren M. Grill, Ph.D.
J. Thomas Mortimer, Ph.D.
Kevin L. Kilgore, Ph.D.
Michael W. Keith, M.D.
David L. Wilson, Ph.D.
Dawn Taylor, Ph.D.
Joseph M. Mansour, Ph.D.
Jeffrey L. Duerk, Ph.D.
Wyatt S. Newman, Ph.D.
Harry Hoyen, M.D.
John Chae, M.D.
Jonathon S. Lewin, M.D.
Dustin Tyler, Ph.D.

Program Manager: William D. Memberg, M.S.

Case Western Reserve University
Wickenden 407
10900 Euclid Avenue
Cleveland, OH 44106-7207
216-368-3158 (voice)
216-368-4969 (FAX)
rfk3@po.cwru.edu

Contract abstract

The overall goal of this contract is to provide virtually all individuals with a cervical level spinal cord injury, regardless of injury level and extent, with the opportunity to gain additional useful function through the use of FNS and complementary surgical techniques. Specifically, we will expand our applications to include individuals with high tetraplegia (C1-C4), low tetraplegia (C7), and incomplete injuries. We will also extend and enhance the performance provided to the existing C5-C6 group by using improved electrode technology for some muscles and by combining several upper extremity functions into a single neuroprosthesis. The new technologies that we will develop and implement in this proposal are: the use of nerve cuffs for complete activation in high tetraplegia, the use of current steering in nerve cuffs, imaging-based assessment of maximum muscle forces, denervation, and volume activated by electrodes, multiple degree-of-freedom control, the use of dual implants, new neurotization surgeries for the reversal of denervation, new muscle transfer surgeries for high tetraplegia, and an improved forward dynamic model of the shoulder and elbow. During this contract period, all proposed neuroprostheses will come to fruition as clinically deployed and fully evaluated demonstrations.

Summary of activities during this reporting period

The following activities are described in this report:

- *Measurement of human upper extremity nerve diameters and branch-free lengths*
- *Intra-operative testing of nerve cuff electrodes and implant tools*
- *A forward dynamic shoulder and elbow model*
- *Command sources for high tetraplegia*
- *Supplemental feedback to enhance myoelectric control in a neuroprosthesis*
- *Wireless data acquisition module for use with a neuroprosthesis.*
- *Percutaneous implementation of myoelectric controlled neuroprosthesis: A case study*

Measurement of human upper extremity nerve diameters and branch-free lengths.

Contract sections:
E.1.a.i Achieving Complete and Selective Activation Via Nerve Cuff Electrodes
E.2.a.i Selective Activation of Elbow and Shoulder Muscles by Nerve Cuff Electrodes

Introduction

The ability to activate selectively peripheral nerve trunk fascicles using nerve cuff electrodes is well established. In the effort to combine several upper extremity functions into a single neuroprosthesis we will use this technology for specific muscle activations. External and internal topography studies of the upper extremity nerves are necessary to identify candidate implant sites. The external study has been reported previously and included measurements of the diameters and branch free lengths of the target nerves in six complete brachial plexus dissections. The results of this study indicated acceptable diameters and branch free lengths at the targeted cuff sites. The goal of the internal study is to obtain accurate fascicle topographies at the targeted areas. To increase the amount of information obtained from the internal studies,

the use of a set of lipophilic dyes that retrogradely diffuse in fixed nerve tissue is being pursued. A method using applied dc electric fields to enhance the diffusion of these dyes has been shown to significantly increase the diffusion velocities of the dyes..

Internal Study Results

Traditional cross-sectioning is largely ineffective as a means to follow fascicles through the length of a nerve. Figure 1 shows the significant amount of change that can be seen in peripheral nerve topography over relatively short distances, and illustrates the difficulty in matching patterns from cross-section to cross-section. Even with high frequency cross-sectioning, mapping fascicles from one slide to the next is, at best, a process of repeated educating guessing. Furthermore, traditional cross-sectioning reveals no information about the location of functional groups at a sub-fascicular level. These factors led us to attempt to use a set of lipophilic dyes that has previously shown to trace fixed nerve fibers.

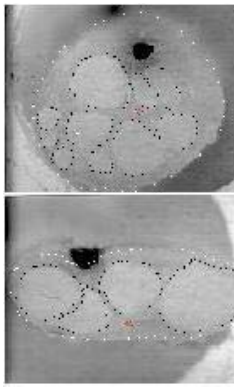

Figure 1. Radial nerve cross-sections 4mm apart.

Retrograde tracing with lipophilic dyes has been used in postmortem formaldehyde fixed nerve fibers (Honig and Hume 1986, 1989; Godement et al. 1987; Honig 1993). The limitation of these dyes is the limited tracing distance that can be achieved due to the slow diffusion rate that is seen in fixed tissue. This slow diffusion rate is due to the cross-linking of proteins that occurs during the aldehyde fixation process (Sparks et al. 2000). Lukas et al. found maximal tracing distance following incubation at 37C for 12-15 weeks of 28.9 ±2.2mm for DiI, with DiO and DiA having maximal tracing distances varying from 15 to 20mm.

Lukas' distances are consistent with other reports and fall well below the distances that would be necessary for our needs. In the radial nerve particularly, tracing distances of at least 150 mm would be desirable, so that we can map the functional groups identified for selective activation at the targeted cuff electrode implantation sites. To overcome this diffusion rate limitation, a method to enhance the diffusion of these dyes has been developed.

This method hinges upon the fact that these three dyes (DiI, DiO, and DiA), as well as an additional analog, DiR, are all positively charged molecules. Theoretically, application of electric fields across the dye-loaded nerve tissue should result in electromotive forces on the molecules driving them through the nerve tissue. To test this theory, two studies were performed. The first of these studies was a time variant study.

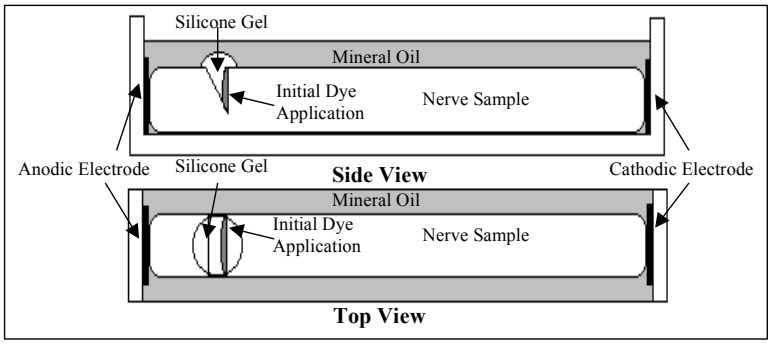

Figure 2. Schematic of Experimental Set-up.

DiI, dissolved in ethanol at a ratio of 1 mg/ml, was applied via a micropipette to a triangular cross-section that was made 1 cm from the end of a 6 cm nerve sample of either human median or ulnar nerves. Platinum plate electrodes were then positioned at either end of the nerve sample, with the electrode closer to the initial DiI loading site serving as the anode (Figure 2).

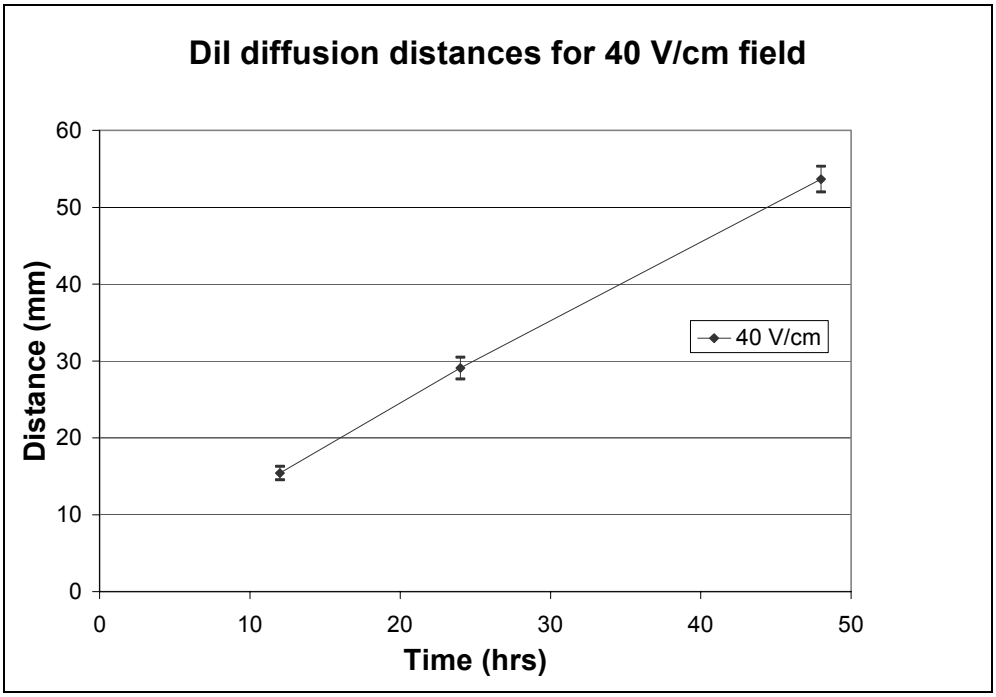

Figure 3. Results of the Time Variance study. Shows maximal tracing distances achieved when applying a 40 V/cm field across DiI labeled tissue for 12, 24, and 48 hours.

A dc electric field of 40 V/cm was applied across the nervous tissue for durations of 12, 24 and 48 hours. Following this tracing period, the nerve sample was embedded in polyacrylamide and cross-sectioned to reveal the extent of DiI diffusion. After analyzing the results, it was determined that the 48 hour trials were limited by the nerve length. They were then redone using 8 cm samples.

The results of this experiment can be seen in Figure 3. The average tracing distances obtained were 15 ± 0.63 mm for the 12 hour trials, 29 ± 1.4 mm for the 24 hour trials and 54 ± 1.7 mm for the 48 hour trials. The average velocity for the entire study was 1.2 ± 0.08 mm/hr. This represents a 158 fold increase over our control samples. The average tracing distance seen in the 48 hour trials corresponds to a 1.86 times increase over the highest reported distances under normal diffusion circumstances (29 mm). This distance increase was achieved in 1.9% of the tracing time that was required for the normal diffusion (15 weeks).

The second study performed was a field variance study. Using the same dye application method, DiI loaded nerves were subject to field strengths of 10, 20, 30, and 40 V/cm for a period of 24 hours.

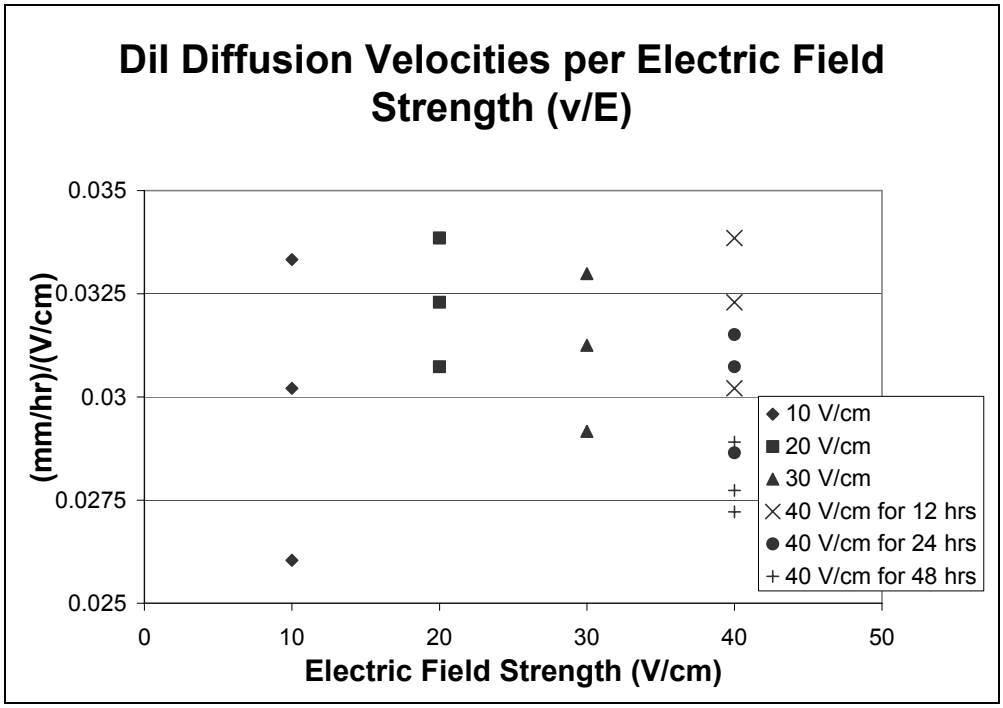

Figure 4. The velocities/electric field strengths for the field variance and time variance studies.

The average velocities obtained at 30, 20, and 10 V/cm were 0.93 ± 0.06 mm/hr, 0.65 ± 0.03 mm/hr, and 0.30 ± 0.04 mm/hr respectively. Combined with the complete results of the time variance study which produced an average velocity of 1.2 ± 0.08 mm/hr, these results demonstrate a very linear relationship between the applied field strength and the resultant diffusion velocity. Figure 4 shows the velocity per electric field values for the results of both the field and time variance studies. The overall average value for this term was 0.031 ± 0.0023 (mm/hr)/(V/cm).

Next Quarter

The use of applied dc fields to overcome diffusion limitations for DiI in fixed peripheral nervous tissue will allow us to create accurate fascicular maps of targeted muscle groups. In the next quarter we will test the efficacy of electric field enhanced diffusion with the other lipophilic dyes.

References

Godement P, Vanselow J, Thanos S and Bonhoeffer F. (1987) A study in the developing visual systems with a new method of staining neurones and their processes in fixed tissue, Development, 101:697-713.

Honig MG. (1993) DiI labeling, Neurosci Protocols 50:1-20.

Honig MG and Hume RI. (1986) Fluorescent carbocyanine dyes allow living neurons of identified origin to be studied in long-term cultures, J. Cell Biol., 103:171-187.

Honig MG and Hume RI. (1989) DiI and DiO: versatile fluorescent dyes for neuronal labeling and pathway tracing, Trends Neurosci., 12:333-341.

Lukas JR, Aigner M, Denk M., Heinzl H, Burian M, and Mayr R. (1998) Carbocyanine Postmortem Neuronal Tracing: Influence of Different Parameters on Tracing Distance and Combination with Immunocytochemistry, J. Histo Cyto, 46(8):901-10.

Sparks DL, Lue L, Martin TA, and Rogers J. (2000) Neural tract tracing using Di-I: a review and a new method to make fast Di-I faster in human brain, J Neurosci Methods, 103: 3-10.

Intra-operative Testing of Nerve Cuff Electrodes and Implant Tools

Contract sections:
E.1.a.i.4.3 Nerve Cuff Electrode fabrication and implantation

Introduction

Self-sizing spiral nerve cuff electrodes [Naples, et al. 1988] will be used to achieve complete activation of paralyzed and partially denervated muscles and produce functionally selective stimulation of multiple nerve fibers within one nerve trunk. These electrodes are self-sizing coils (Figure 5) with four contacts that can be controlled individually to selectively activate one portion of the nerve. The natural coiling of these electrodes is essential for obtaining a snug fit while not compressing the nerve, but also makes them awkward and time-consuming to implant. A custom tool is being designed to facilitate the implant process. This quarter, prototype tools and cuff electrodes have been tested intra-operatively, during brachial plexus and other upper extremity nerve exposure surgeries.

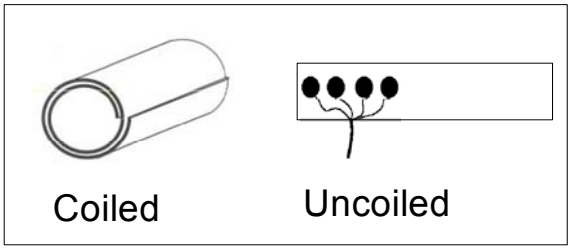

Figure 5. Left – Spiral electrode coiled, resulting in two full wraps. Right – Electrode uncoiled to show contacts.

The nerve cuff electrodes were tested intra-operatively during surgeries of the brachial plexus. This procedure was chosen for several reasons. Most nerves of the shoulder and arm originate in the brachial plexus. A brachial plexus injury usually results in damage to some, but not all, of these nerves. Surgeons use evoked potential tests to examine nerve viability and guide repair strategies. They place an electrode on the target nerve, stimulate, and measure the evoked cortical and electromyography (EMG) signals. In addition to the conventional electrode, surgeons are using nerve cuff electrodes intra-operatively to stimulate the target nerves. The

purpose of intra-operative testing is to assess prototype tools, determine cuff stimulation parameters, and become familiar with the cuff and implant tool.

Methods

Tool Design: Design specifications (Table 1) for a nerve cuff implant tool were derived from discussions with surgeons, engineers and investigators familiar with cuff implantation.

Problem	**Approach**
The corners of the cuff curl in when held in the center or at one side.	Hold the cuff at both corners.
Lowest thresholds are obtained when the cuff fits snugly around the nerve.	Hold one end securely and apply tension to the loose end.
Tool holds the inner wrap of the cuff; consequently, outer wrap covers tips.	Separate the tips for removal of tool without pulling cuff.
Nerve exposure may be limited and deep.	Make tool long and thin.
The nerve is surrounded by other tissue.	Include a mechanism to cradle and gently lift nerve.
The cuff will be loaded into the tool by an assistant.	Make forceps normally closed for easy transfer between assistant and surgeon.
The surgeon needs to wrap the cuff around the nerve.	Create adequate space around the cuff.
Assistance shouldn't be required to implant electrode.	Facilitate one-handed installation.

Table 1. Design challenges and possible approaches

The initial prototype (Figure 6) was developed to test design concepts with minimal cost. Two bayonet shaped forceps (21 cm long) were custom bent at the tips. This brought the tips together and enabled them to grip the corners of the cuff. The forceps were held in a normally closed position by a silicone ring. Rotating a stainless steel tab opened the tips. A silicone spacer maintained constant tip separation during loading and cuff installation.

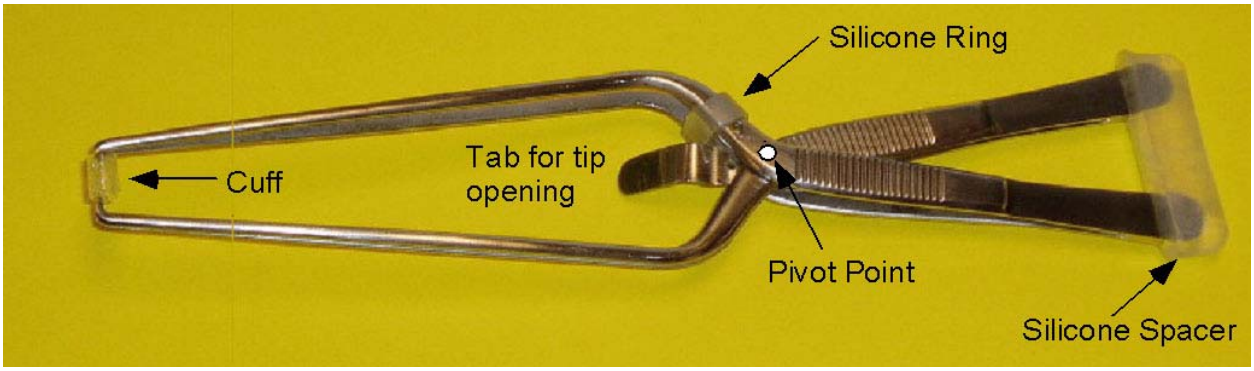

Figure 6. Tool used during first intra-operative test.

There are three primary functions of the tab and silicone spacer (Figure 7). When the tab is in the central position, the tips are held closed (see Figure 7A). When the tab is rotated, the tips open enough to allow the cuff to be loaded or released (Figure 7B). When the silicone spacer is removed, the tips separate (Figure 7C) so that the tool can be removed from the site without pulling the electrode.

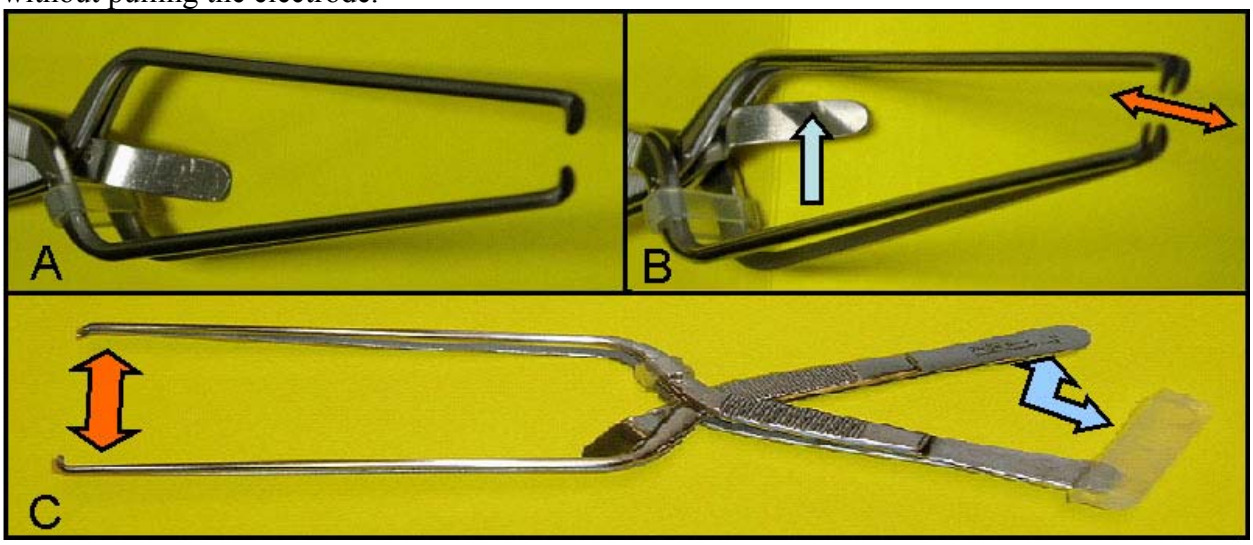

Figure 7. Functions of tab and silicone spacer. (A) Tab centered allows tips to be in normally closed position. (B) Rotating the tab causes tips to open. (C) Removal of the silicone spacer allows the tips to separate.

Implantation of the nerve cuff using the prototype tool consists of five main steps (Figure 8). An assistant loads the cuff into the tool (see Figure 8A). The surgeon unrolls the cuff and holds it under the nerve (Figure 8B & 8C). Using strongly bent forceps, the surgeon wraps the cuff around the nerve, applying tension to obtain a snug wrap (Figure 8C & 8D). Before removing the tool from the site, the tips are opened (tab rotated) and separated (spacer removed) to release the cuff (Figure 8E).

***Intra-Operative Testing*:** During brachial plexus repair surgeries, the surgeon stimulated different portions of each nerve while recording EMG, brainstem and cortical responses. Approval was obtained from the MetroHealth Medical Center Investigational Review Board to perform this stimulation with both a conventional electrode and a spiral nerve cuff electrode. An investigator loaded the cuff electrode into the implant tool and passed the tool to the surgeon. The electrode was placed around the nerve and connected to a stimulator. Both the time to load the cuff into the tool and the time to implant the cuff around the nerve were recorded to evaluate the tool. Surgeon comments were also noted.

Each nerve was stimulated with the cuff to determine the parameters required to produce a response. The current threshold was determined by fixing the pulse width and increasing the pulse amplitude by 0.1 mA until a response was observed.

Results

One subject has been enrolled. The nerve cuff was successfully placed on three nerves in this subject. The surgeon used the implant tool on two nerves but did not use it on the third. The implant time was two minutes or less while using the implant tool and around four minutes without the tool (Table 2).

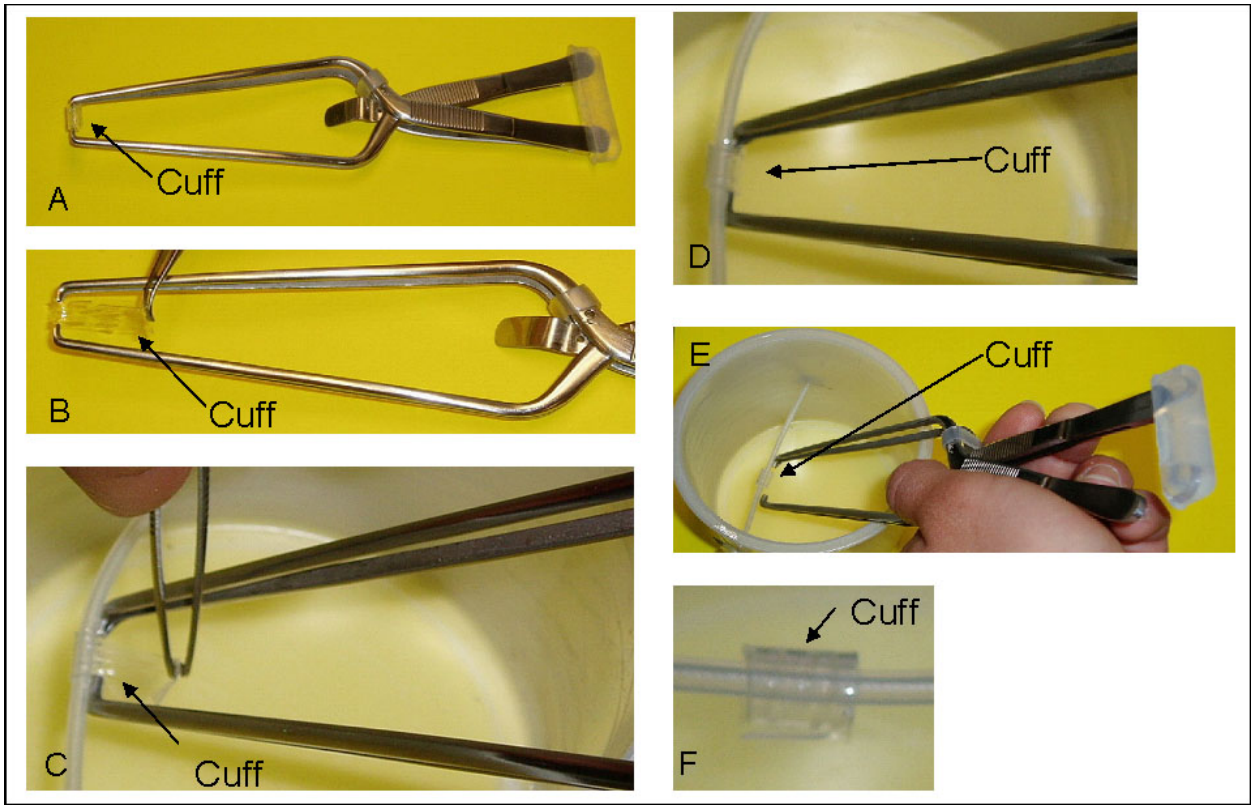

Figure 8. Steps to Cuff Implantation. (A) Load cuff into tool. (B) Unroll cuff. (C) Hold cuff under nerve; wrap around nerve using forceps. (D) Cuff snuggly wrapped, twice around. (E) Open and separate tips to release cuff. (F) Cuff implanted.

Qualitative results from the tool testing are:

- The implant tool firmly held the cuff in place during cuff installation and was successfully removed by tip opening and separation.
- An assistant was required to install the cuff. The surgeon held the implant tool with one hand. Wrapping the cuff around the nerve required his other hand and the help of an assistant.
- The tool was too wide for the small incision of one site.

The surgeon suggested including a bend in the tool that allowed it to easily slide under the nerve, and developing a method to facilitate wrapping.

Nerve	Implant Time	Tool	Diameter	Parameters	Comments
Phrenic	2 min	Y	1.5 mm	100 us, 1.7 mA	Motor response observed, did not find threshold.
C8	1 min	Y	>4	N/A	Nerve avulsed.
Spinal Accessory	~4 min	N	1.5-2 mm	100 us, 1 mA	Cortical response – cuff fit loosely and threshold decreased when surgeon improved the fit
				50 us, 2 mA	

Table 2. Results of cuff implantation.

Very little motor response was observed from any nerve because most of the brachial plexus (C5-C7) was avulsed. Stimulation of the phrenic nerve did result in diaphragm contraction but threshold current was not found due to time constraints. Stimulation of the eighth cervical nerve produced no response even at high current levels. The current threshold of the spinal accessory nerve was found at pulse width values of 50 and 100 microseconds (Table 2).

The cuff electrode available for these tests was designed to fit snuggly around 4 mm diameter nerves even though the nerves tested varied in size. One of the nerves tested was larger than 4 mm, while two were significantly smaller. A larger diameter nerve resulted in less cuff overlap but still obtained a snug wrapping. Smaller nerves did not fit snugly in the cuff and there was poor contact between the electrode and the nerve. On the spinal accessory nerve (diameter ~2 mm), the surgeon was able to decrease the current threshold of the response by applying pressure to the cuff. This improved the contact between the electrode and the nerve, simulating a snug fit.

Discussion

During discourse with the surgeons, it was suggested that tabs be added to the edges of the cuff, near the contacts, to eliminate the need for the tips to separate. This greatly simplified the tool design (Figure 9). The 'U'-shaped design allows for adequate room around the cuff, is in a normally closed position and can be operated with one hand. This design also includes a bend at the end to cradle the nerve above the surrounding tissue.

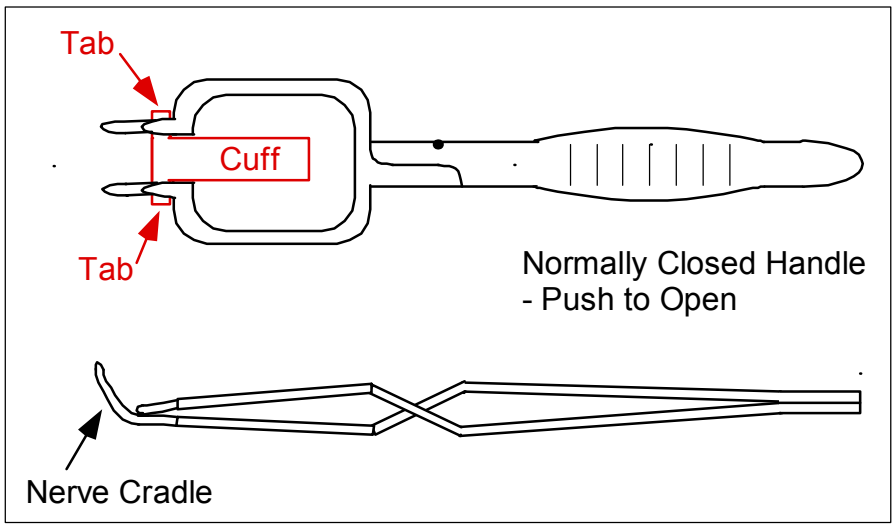

Figure 9. Next generation implant tool design.

While installation time was short, a mechanism to facilitate wrapping the cuff around the nerve is needed to eliminate the need for assistance. Currently, the surgeon feeds the end of the cuff under the nerve with his free hand and requires a surgical assistant to pull the cuff over the nerve. It is desirable for the tool to have a mechanism to push the cuff under the nerve so the surgeon can grab the end with his free hand and complete the installation.

The stimulation levels needed to evoke a response during the intra-operative testing session were much higher than previous values of cuff stimulation in cats [Grill and Mortimer 1996; Grill and Mortimer 1996; Grill and Mortimer 1998]. This could be due to the large cuff

diameter to nerve diameter ratio, but pressing on the cuff did not significantly reduce the required current. Also, all of the nerves tested were injured and were not necessarily as excitable as healthy nerves. Finally, the response was predominantly sensory, not motor. The cortical and brainstem responses are recorded using corkscrew and subdermal electrodes. This recording method could affect the apparent threshold of the nerve cuffs since it is unable to detect small ENG activity. In order to develop an implantable stimulator, the stimulation parameters of human motor neurons are needed. These preliminary results indicate higher current requirements than observed in animal models. It is important to establish whether this is an artifact of the surgeries chosen or is to be expected.

Next Quarter

Goals for the next quarter include:

- Fabricate and test the next generation implantation tool.
- Develop and test a cuff wrapping tool.
- Finish the intra-operative testing of the implantation tool and cuff.
- Implant in a human the first set of nerve cuff electrodes with a percutaneous interface.

References

Grill, W. M., Jr. and J. T. Mortimer (1996). "The effect of stimulus pulse duration on selectivity of neural stimulation." IEEE Trans Biomed Eng **43**(2): 161-6.

Grill, W. M., Jr. and J. T. Mortimer (1996). "Quantification of recruitment properties of multiple contact cuff electrodes." IEEE Trans Rehabil Eng **4**(2): 49-62.

Grill, W. M. and J. T. Mortimer (1998). "Stability of the input-output properties of chronically implanted multiple contact nerve cuff stimulating electrodes." IEEE Trans Rehabil Eng **6**(4): 364-73.

Naples, G. G., J. T. Mortimer, et al. (1988). "A spiral nerve cuff electrode for peripheral nerve stimulation." IEEE Trans Biomed Eng **35**(11): 905-16.

A Forward Dynamic Shoulder and Elbow Model

Contract section: E.1.a.ii.4.3 Development of forward dynamic model of human arm

Introduction

In order to restore function to individuals with high tetraplegia (C4), an upper extremity neuroprosthesis is under development. This is a system that combines functional electrical stimulation (FES) with reconstructive surgeries, like tendon transfers or fusion of specific articulations [Keith and Lacey, 1991]. The FES system consists of a controller that outputs the muscle excitations needed for a particular task and electrodes that are used to deliver the stimulation to the appropriate paralyzed muscles. To guide the development of the upper extremity neuroprosthesis, a computer model of the shoulder and elbow has been built. An important advantage in using a musculoskeletal model is that it allows the relatively easy and fast evaluation of surgical techniques, minimizing the inconvenience to the subjects. There are a large number of shoulder and elbow muscles that must be controlled in individuals with high level spinal cord injury, many of which generate moments about two or more degrees of

freedom. Therefore, purely experimental methods are often inefficient and impractical for developing, testing, and tuning a controller that produces appropriate responses to user commands and external disturbances. Our approach is to use a musculoskeletal model as a substitute for the real human arm in order to evaluate different strategies for control system design.

A musculoskeletal model is a mathematical representation of a musculoskeletal system, a complex biological structure that usually includes bones, muscles, tendons, ligaments and joints. Most systems contain multiple segments connected by different types of joints. The movement of these limb segments is described by a set of differential equations, called the equations of motion, that connect the segment positions, velocities and accelerations to the forces that act on them and cause the movement. Even for a relatively simple musculoskeletal model, these equations are too complicated for a practical analytical solution to be derived, so a numerical solution is usually found with the use of a computer.

The shoulder mechanism is a very complex system. Since the upper extremity is used for manipulation rather than for support of body weight or locomotion, a wide range of motion is advantageous. This is provided by the shallow cavity of the glenoid that allows the humerus to move almost without bony constraints. Further mobility is provided by the closed-chain mechanism consisting of the scapulothoracic gliding plane, the interface between the scapula and the thorax, and the sternoclavicular and acromioclavicular joints. Stability of the glenohumeral joint (i.e., maintaining the proper relationship between the humeral head and the glenoid socket) and of the scapula (i.e., maintaining the scapula flat against the thorax) are primarily provided by muscular rather than skeletal or ligamentous actions. There are seventeen muscles crossing the three shoulder joints, many of which cross more than one of these articulations, have large attachment sites, and contain multidirectional muscle bundles [van der Helm, 1994].

Van der Helm mentioned that the first shoulder models were physical models that were built using human specimens by Mollier (1899), Shiino (1913) and Hvorslev (1927). The first mathematical models were two-dimensional, were restricted to single-motion patterns, and did not include all the shoulder muscles [DeLuca and Forrest 1973, Dul 1987]. There are very few three-dimensional models, probably because of the complexity of the shoulder mechanism. The "Swedish" shoulder model was developed by Karlsson and Peterson, based on morphological measurements by Hogfors et al. [Karlsson and Peterson 1991, Hogfors et al. 1987]. The "Dutch" model, by van der Helm, is based on morphological data from Veeger et al. [van der Helm and Veenbaas 1991, van der Helm et al. 1992, van der Helm 1994, Veeger et al. 1991, 1996, 1997]. It uses the computer program SPACAR, a software program that implements a finite element method and is specifically suited for analysis of multibody systems [Van Soest et al. 1992]. The "Newcastle" shoulder model, described by Charlton and Johnson, is based on data from Johnson et al., van der Helm and Veeger [Charlton and Johnson 2000, Johnson et al. 1996, van der Helm et al. 1992, Veeger et al. 1997]. It uses SIMM (Software for Interactive Musculoskeletal Modeling, Musculographics Inc), a graphics-based software system that allows users to develop, analyze, and visualize musculoskeletal models [Delp and Loan 1995].

As was already mentioned, one of the complicating factors in modeling the shoulder is the broad muscle attachment sites that cannot be realistically modeled by a single line of action. For example, the trapezius is a broad pennate muscle, whose lower fibers act with a significantly different angle than the fibers of the upper part. In earlier shoulder models, this problem was solved by dividing the broad muscles into independent parts, based on functional or anatomical criteria, and each part was represented by a separate line of action [DeLuca and Forest 1973,

Poppen and Walker 1978]. This approach was made more systematic by van der Helm and Veenbaas, who developed a method for the derivation of the muscle lines of action [van der Helm and Veenbaas 1991]. The aim was to minimize the number of force vectors required to represent each muscle, while keeping the error in the mechanical effect negligible. This method was implemented in the Dutch model. Charlton and Johnson divided the large muscles based on anatomical criteria, while Karlsson and Peterson used functional criteria, derived from the measurements of Hogfors et al. (1987).

For most of the shoulder muscles, the actual line of action is not straight, since the muscles cross one or more joints and wrap around bone surfaces. Hogfors et al. dealt with this problem by adding points along the muscle ("virtual origins") to better define curved muscle lines of action [Hogfors et al 1987]. Charlton and Johnson used SIMM's inherent muscle-wrapping capabilities, although the version of SIMM used did not allow wrapping around more than one object, a capacity that has been added in newer versions [Charlton and Johnson 2000]. In the Dutch model, the bony contour method was used, which means that the muscle line of action was defined as the shortest distance between the origin and insertion around the bony contour that is in between. This line was represented in SPACAR by a special curved-truss element [van der Helm 1994].

Most of the musculoskeletal models of the shoulder developed to date are inverse models, meaning that their inputs are the joint angles and external forces, and their outputs are the required muscle forces. Since there are more muscles than degrees of freedom, estimating the muscle forces is an indeterminate mechanical problem that is solved using optimization techniques. The objective functions most commonly used are the sum of muscle stresses, or the sum of squared or cubed muscle stresses. Karlsson and Peterson reported that they used the sum of squared stresses after they compared powers of 1.5, 3 and 4 and concluded that they do not differ very much [Karlsson and Peterson 1991]. Van der Helm compared four different objective functions: the sum of quadratic muscle forces, the sum of quadratic muscle stresses, the sum of quadratic muscle forces normalized to the maximal muscle force, and the maximal muscle stress in the entire mechanism. His conclusion was that minimization of the sum of quadratic muscle stresses is the preferred criterion, because it takes into account the physiological cross sectional area and is computationally efficient [van der Helm 1994]. The same technique was used in the Charlton and Johnson model [Charlton and Johnson 2000].

Because of the complexity of the shoulder mechanism, there are certain constraints that need to be added to the optimization routines in order to achieve realistic force balance. In the Dutch model, scapular stability is insured by requiring the scapula to be pressed against the thorax at all times, i.e., the force on the scapulothoracic gliding plane is constrained to zero or negative (compression). Ligaments can produce force only in tension, so stress in the conoid ligament is restricted to zero or positive. Glenohumeral stability is guaranteed by requiring the net glenohumeral reaction force vector to point into the glenoid cavity. Otherwise the joint would dislocate [van der Helm 1994]. The importance of this constraint for the stability of the shoulder can be seen in the Swedish model: no constraint for the direction of the glenohumeral contact force was included, and this created a significant tendency for subluxation [Karlsson and Peterson 1991].

When the inputs to the model are the muscle activations and the outputs are the joint positions, velocities and accelerations, this is called a forward simulation [van den Bogert in Nigg 1999]. Optimization of forward models is extremely cumbersome, because unlike inverse simulations where the optimization problem can be solved independently for each time step, in

the forward simulations every neural input has to be optimized in time. Proper muscle activations need to be determined so that the constraints of the shoulder mechanism are not violated (i.e. the scapula stays attached to the thorax and the humeral head stays in the glenoid cavity). The only forward model of the shoulder developed to date was created by van der Helm and Chadwick. To solve this problem, they developed an algorithm that sets boundaries for the neural inputs by using an inverse muscle model [van der Helm and Chadwick 2003].

Another difficulty with the forward model is that the equations of motion are not algebraic equations that can be easily solved, but instead they need to be integrated, which is computationally demanding. In the van der Helm and Chadwick model, two integration algorithms were tested: an Adams-Moulton algorithm (a variable-order, variable step-size predictor-corrector algorithm), and the Euler integration algorithm (which requires only one function evaluation per integration step). This is the simplest integration algorithm, but its accuracy depends on the predefined integration step size. It was determined that the Adams-Moulton and a 1 msec Euler algorithm gave similar results.

The only forward model of the shoulder and elbow that is currently available, created by van der Helm and Chadwick (2003), is still under development and has very slow simulation speed. Moreover, the software package used to implement the model is not widely used and is not user-friendly.

The purpose of this project was to create a forward dynamic model of the shoulder and elbow with a graphical interface, using commercially available software packages. With the addition of optimization routines, this model can also be used for inverse dynamic simulations, thus providing a complete description of the shoulder and elbow.

Methods

The software used to create the model is SIMM (Software for Interactive Musculoskeletal Modeling, Musculographics, Inc.), a graphics-based system developed especially for musculoskeletal modeling. SD/FAST is a separate software system available from Parametric Technology Corp. that uses parameter files created by SIMM to define the model structure and to compute the equations of motion of the modeled system. The Dynamics Pipeline is a suite of software subroutines available from Musculographics, Inc. that connects SIMM to SD/FAST in order to create the model subroutines and to perform forward and inverse simulations.

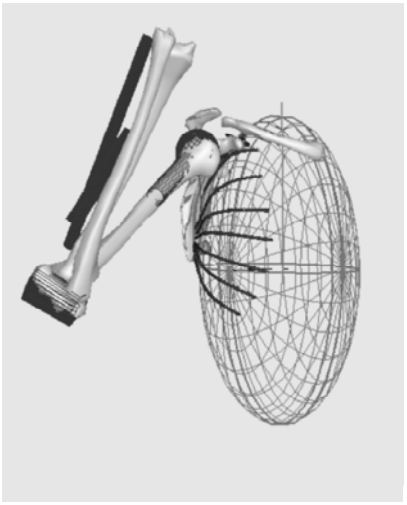

Figure 10. Example of the representation of a broad muscle, the serratus anterior.

The input to SIMM is a set of files describing the joints, muscles and bones. The degrees of freedom and the coordinate frames were chosen here to follow the protocol proposed by the International Society of Biomechanics, the International Shoulder Group and the Delft University group (see appendix A). The muscle and joint parameters previously obtained by the van der Helm group [van der Helm and Veenbaas 1991, van der Helm et al. 1992, van der Helm 1994, Veeger et al. 1991, 1996, 1997] were transferred directly into the SIMM environment.

The *muscle* file contains the geometry and the force-generating properties of the muscles. Each muscle is represented by one or more elements, depending on its size and the width of its attachment site. Figure 10 shows a lateral view of the model with 12 muscle lines representing the serratus anterior, originating from the upper 8 ribs and inserting at the scapula. A list of the muscles and the number of elements that model each one is included in appendix B. The geometry of a muscle is defined by a series of attachment points connected by line segments. At least two points are required to define the muscle path, fixed to one of the body segments. If the muscle wraps over a bone surface, a wrap object is used to represent that surface, such that the muscle path is not allowed to go through the bone. In Figure 11, the spherical wrap object representing the head of the humerus is shown. The long head of the biceps goes over this object from its origin on the scapula to its insertion on the radius. The wrap objects are actually defined in the joint file, but the muscle needs to be associated with the object it wraps around, by specifying it in the muscle definition. Ligaments are modeled in SIMM as muscles that have fibers of zero length and no active force properties. Like muscles, they can cross any number of body segments, and can wrap over wrap objects.

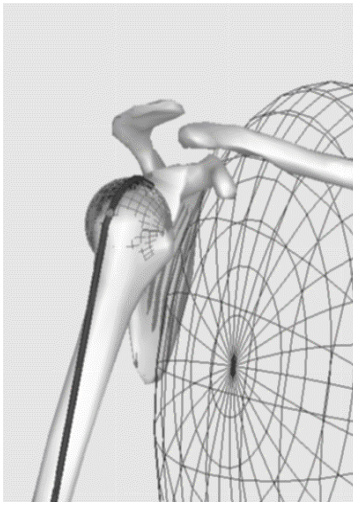

Figure 11. Example of wrapping: the long head of biceps over the humeral head.

The isometric force-generating properties of a specific muscle are derived by scaling a generic, Hill-based model. To scale the generic model, four parameters and three curves need to be supplied. The four parameters are the peak isometric muscle force, optimal muscle-fiber length, pennation angle, and tendon slack length. The three curves are the active and passive force-length relations of muscle, and the force-length relation of tendon. The force-velocity characteristics of the muscle-tendon actuators can also be modeled if the maximum contracting velocity and the force-velocity curve are supplied.

The *joint* file contains the definition of the body segments, joints, degrees of freedom, muscle wrap objects and constraint objects. A body segment consists of one or more bones fixed in a reference frame, and two bodies are connected in any arrangement by defining joints. The transformations from one body segment to the next are either rotations or translations, and they are either constant or a function of one of the degrees of freedom. The degrees of freedom of this model are included in appendix A. The only constraint object in this model is an ellipsoid representing the thorax. Two points on the scapula, determined by the Van der Helm group, stay connected to the thorax at all times, thus implementing the scapulothoracic gliding plane. This is shown in Figure 12: the two spheres are the points on the scapula and the ellipsoid is the thorax, on which they are constrained.

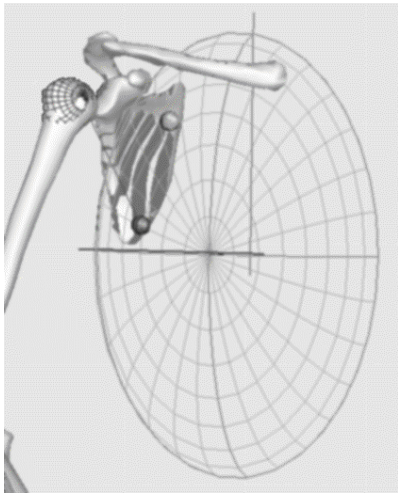

Figure 12. The scapulothoracic gliding plane constraint.

The last set of files is the *bone* files, which contain lists of polygons defining the bone surfaces. A general model of the upper body skeleton was used, scaled to match the dimensions of the cadaver. Precision is not required when creating the bones, because they are merely visual aids for moving the joints and placing the muscles, and they are not necessary for developing and analyzing models in SIMM.

The above parameters are needed to specify a musculoskeletal model in SIMM. For the SIMM model to be used with the Dynamics Pipeline, however, several dynamic parameters must also be specified. In the joint file, each of the body segments needs to include the mass, center of mass, and moments of inertia with respect to the mass center, along the axes of the segment's reference frame. In the muscle file, if a muscle is to be activated in the dynamic stimulation, its excitation pattern needs to be specified. Excitation is defined as the control signal to the muscle and ranges from 0 (no excitation) to 1 (full excitation). In order to calculate the activity level of the muscle fibers ("activation") in response to an excitation pattern, the activation and deactivation time constants need to be added in the muscle file. Finally, a parameter specifies which of several available muscle models should be used to calculate muscle force. The Dynamics Pipeline has seven built-in muscle models, all based on a Hill-type model but including different parameters (i.e. activation, fiber length, fiber velocity and combinations of these) that affect their accuracy and computational efficiency.

The model used in the simulations presented in this report is a one-state model created for computational speed by Felix Zajac, at Stanford University, and only takes activation into account:

$$F(t) = F_o\, \alpha(t) \cos\theta$$

where F is the muscle-tendon force, F_o is the maximum isometric force, α is the activation level and θ is the pennation angle.

The simplest model was used here to insure that the verification of the mechanical structure of the musculoskeletal model was not complicated by the presence of muscle dynamics. It is straightforward to include more complete muscle models.

Two output files are created each time a forward dynamic simulation is performed: a motion file and a kinetics file. A SIMM motion file includes the joint angles, muscle activations, forces, and lengths generated by the simulation. This file can be loaded into SIMM to replay the simulated motion and any of the data in the file can be plotted. The kinetics file, which is intended to provide the data needed to perform an inverse dynamic simulation with the model, includes joint angles, velocities and accelerations.

SD/FAST computes the equations of motion, and it can be used to perform analysis on any mechanical system, not just a musculoskeletal model. All the properties of the system are passed to SD/FAST in the System Definition File, which is supplied by the user, and it results in the generation of a problem-specific source-code numerical model. This means that instead of using generic equations, SD/FAST uses the parameters of the particular model to apply simplifications and derive the simplest possible equations of motion, resulting in high speed performance. The outputs of SD/FAST include the angular and translational locations, velocities and accelerations of any body segment, point, or joint axis in the system, expressed in any reference frame.

The Dynamics Pipeline connects SIMM to SD/FAST in order to run dynamic simulations. SIMM creates C code implementing the kinematics of the joints in the model, SD/FAST creates C code implementing the equations of motion for the body segments, and the

Pipeline library contains code that sets up the simulation and implements the equations of motion for the muscle-tendon actuators. The interactions between the software packages are illustrated in Figure 13. A forward dynamics analysis involves computing the motions of the body segments, given the forces and torques acting on the system. The equations of motion for the system are first derived, and then they are integrated over a specified time period to calculate the body segment motions. The integration routine used is a variable-step method based on a fourth order Runge-Kutta-Merson.

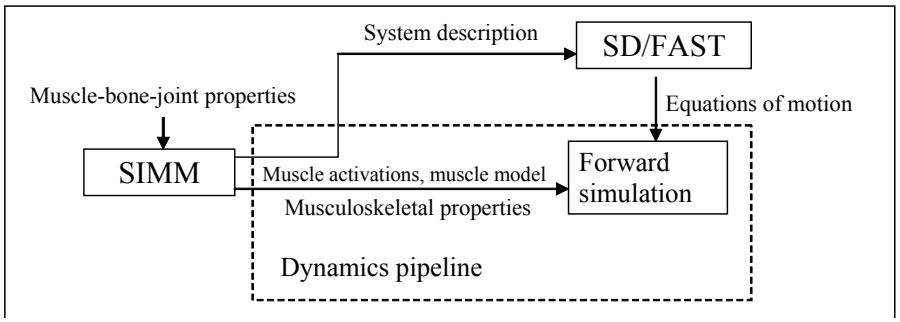

Figure 13. A diagram illustrating the interactions between the software packages needed to run a forward dynamic simulation.

Results

Model construction. The model was constructed as described in the Methods section, with significant assistance from Peter Loan of Musculographics, Inc. and Edward Chadwick from the Delft Shoulder Group. In order to use the muscle and joint parameters measured by the van der Helm group, certain transformations and adjustments needed to be made. The positions of the bony landmarks, joint centers of rotation, and muscle origins and insertions were defined in the global coordinate frame in the van der Helm model. These were translated into the local coordinate frames of the segments in order to be used by SIMM. The effectiveness of the wrap objects was tested by moving the joints through their entire range of motion and checking the line of action of individual muscles. This resulted in small changes in the coordinates of certain muscle points, like the origin of the pronator quadratus that was incorrectly wrapping around the ulna in extreme supination.

Model verification: shoulder. Preliminary evaluation of the basic mechanical structure of the model was performed through a series of forward simulations. As indicated above, a static muscle model was used, but otherwise the simulations included inertia effects and first order activation and deactivation time constants and were thus dynamic. No external loads were applied to the arm – the simulated muscle forces acted only on the weight and inertial properties of the arm. Using single muscle excitations as input, the resulting joint angles were compared to those expected from the action of each muscle. For example, excitation of the brachialis is known to produce elbow flexion, and this was confirmed by simulating activation to the brachialis only and verifying that elbow flexion resulted. In this way, the actions of all the muscles were checked individually. In another set of simulations, more than one muscle was activated at the same time, in order to demonstrate the complicated but known relations between different muscle groups.

In the first part of this section, the effect of various muscles on the humeral abduction angle is investigated. It should be noted that in the real system, many more of the shoulder muscles would take part in this apparently simple movement, with activation patterns that vary greatly with time. For the purposes of this example, the excitation patterns are assumed to be step functions, and only the muscles with the greatest relevance to humeral abduction were examined.

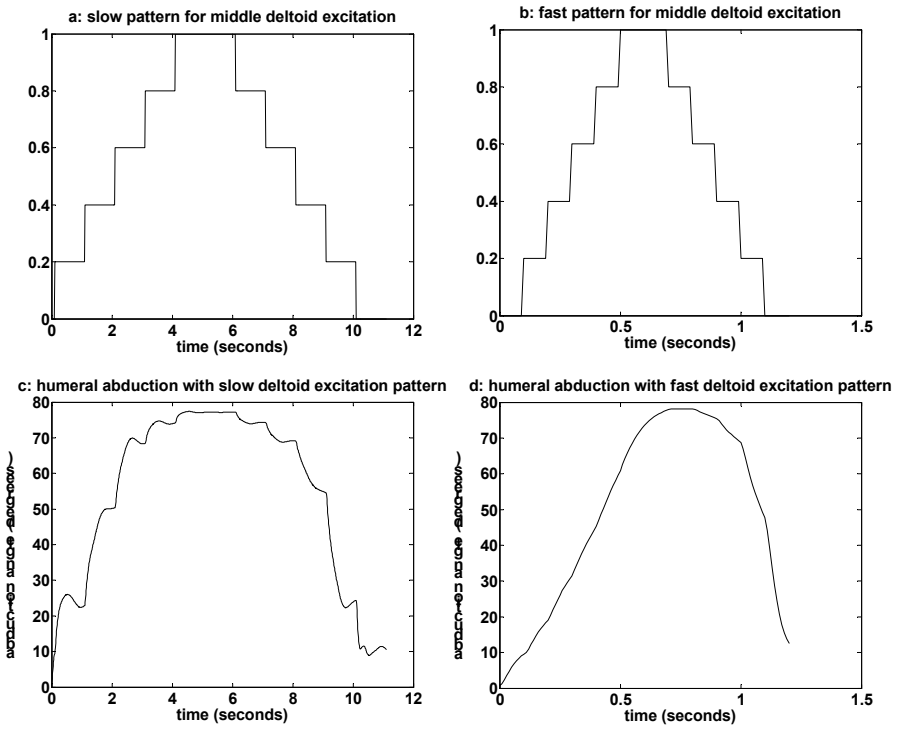

Figure 14. Effect of activation dynamics on humeral abduction.

Figure 14 illustrates the effect of inertia and activation dynamics on the time course of the shoulder abduction angle. The only muscle activated was the middle (lateral) deltoid, and two different excitation patterns are used, shown in Figures 14a and 14b. The resulting abduction angle is illustrated in Figures 14c and 14d respectively.

As expected, activation of the middle deltoid produced glenohumeral abduction for both temporal patterns. When the fast excitation pattern was applied (Figure 14b), the excitation level changed every 0.1 second, while in the slow pattern (Figure 14a) it changed every 1 sec. Note that the increase in abduction angle was much smoother with the fast excitation pattern.

Figure 15 illustrates the relationship between excitation and activation, which is approximated by a first order differential equation. A simple step is used as the excitation pattern, and the resulting activation is plotted for one of the elements of the middle deltoid. The increase in activation is much faster than the decrease, reflecting the smaller time constant for activation relative to deactivation.

Figure 16 illustrates the time course of the shoulder abduction angle as two muscles that have significant abduction actions on the humerus are independently activated: the middle deltoid and the supraspinatus. The same excitation pattern was used for both muscles. As expected, progressive increases in the excitation of the middle deltoid resulted in progressive increases in abduction angle up to a maximum of approximately 78 degrees at full excitation. The supraspinatus produced a maximum abduction

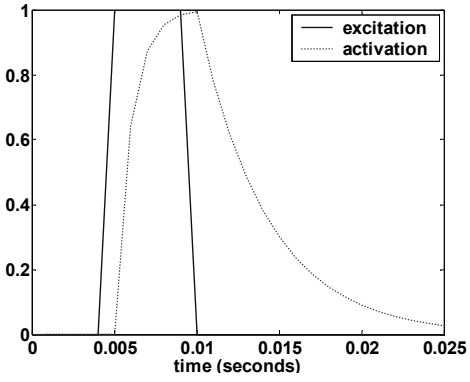

Figure 15. Activation dynamics.

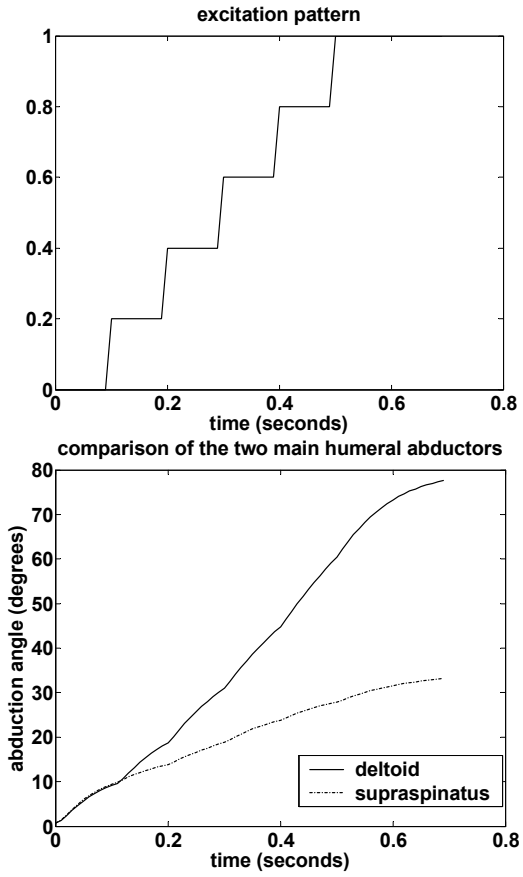

Figure 16. Effects of middle deltoid and supraspinatus on humeral abduction angle.

angle of 32 degrees, reflecting its known role as a secondary shoulder abductor.

Figure 17 illustrates the incremental increase of shoulder abduction angle provided by adding a constant 0.8 excitation of the upper and lower parts of the trapezius to the progressive activation of the middle deltoid. Note that constant trapezius excitation levels ranging from 0.2 to 1.0 were examined, and the largest effects on shoulder abduction were seen for excitations greater than 0.6. Including trapezius excitation increased shoulder abduction angle from 78 to 121 degrees, indicating the important role of trapezius in shoulder abduction, mediated via its actions on the scapula.

Model verification: elbow. Similar simulations were performed to verify the actions of several elbow muscles. Figure 18 shows the elbow flexion angle generated by individual excitation of both heads of the biceps (solid line), brachialis (dash-dotted line), and brachioradialis (dashed line). The arm began at the side and the forearm was in a semiprone position (-90 degrees of the PS y degree of freedom). All three muscles moved the elbow into flexion as expected. The brachialis produced the largest maximum flexion angle (108 degrees) while the biceps produced the smallest maximum angle (80 degrees).

Figure 19 illustrates the results of simulations that were similar to those used in Figure 17, except that the initial position of the forearm was at full pronation (0 degrees of PS y), and a constant excitation 0.8 of the pronator teres and pronator quadratus was used during the entire simulation in order to keep the forearm pronated. Overall, the three flexor muscle responses were very similar to those achieved for the semiprone position, but the brachioradialis produced a slightly smaller maximum flexion angle (80 degrees versus 85 degrees).

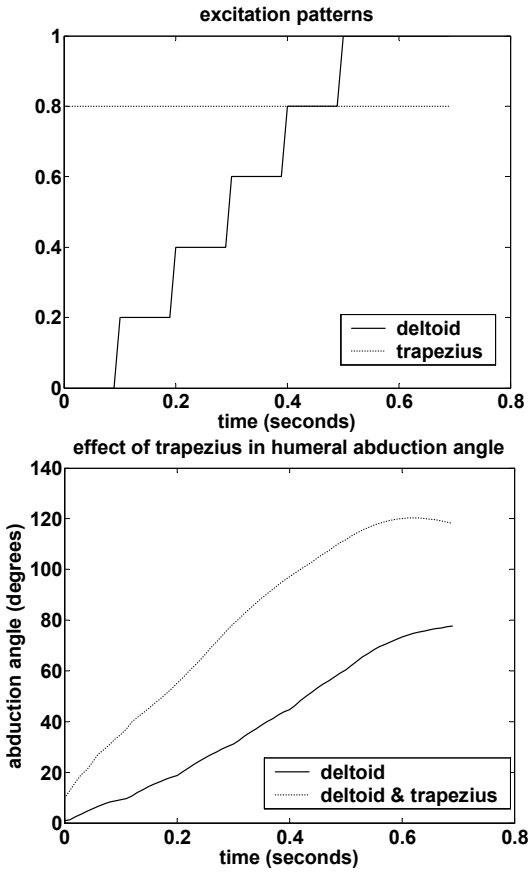

Figure 17. Effects of upper and lower trapezius excitation on humeral abduction angle.

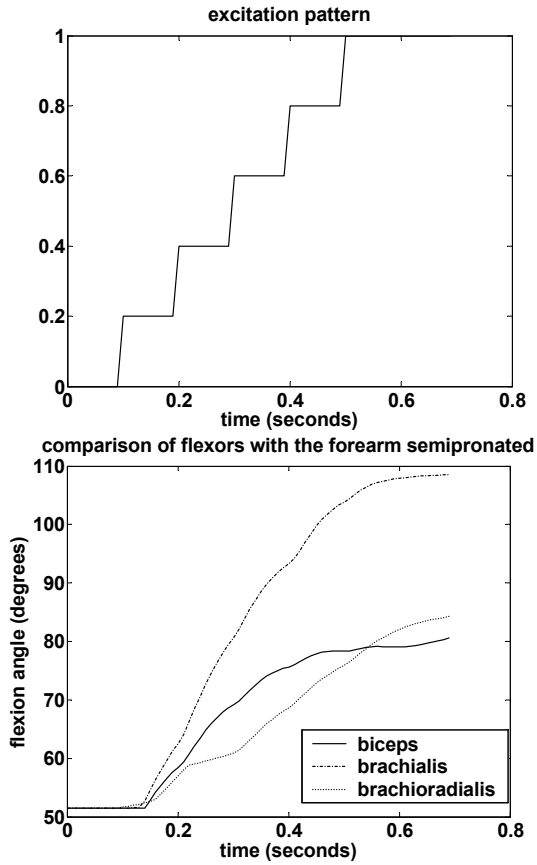

Figure 18. Effects of biceps (both heads), brachialis, and brachioradialis excitation on the elbow flexion angle when the forearm is in the semiprone position.

Figure 20 shows the results obtained or a fully supinated position (-160 degrees of PS y). In this case, constant excitation 0.8 of the supinator ensured that the forearm remained supinated. The flexor muscle responses were again similar to those obtained for other forearm orientations, although the maximum flexion angle produced by biceps increased from 80 to 88 degrees relative to the pronated orientation.

Discussion

A forward dynamic model of the upper extremity has been described. It was developed using a set of commercially available software packages and it incorporates the geometrical and force parameters calculated from cadaver measurements by van der Helm et al. at the University of Delft. The use of the model was demonstrated in a series of forward simulations with activation of several different muscles. These are simple demonstrations that certainly do not provide an exhaustive validation of the model. However, the simulations produced joint angle trajectories qualitatively similar to those expected from these muscles, indicating that the structure of the model is correct.

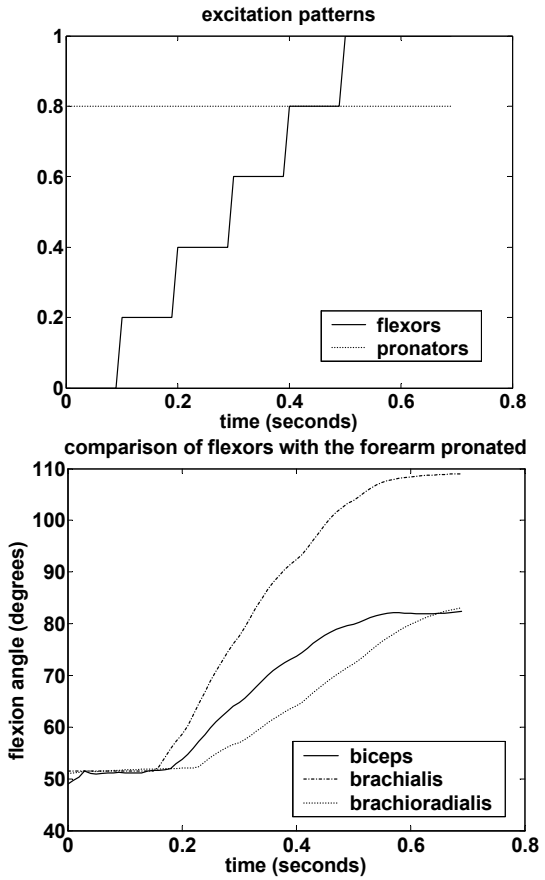

Figure 19. Effects of biceps (both heads), brachialis and brachioradialis on elbow flexion angle when the forearm is fully pronated.

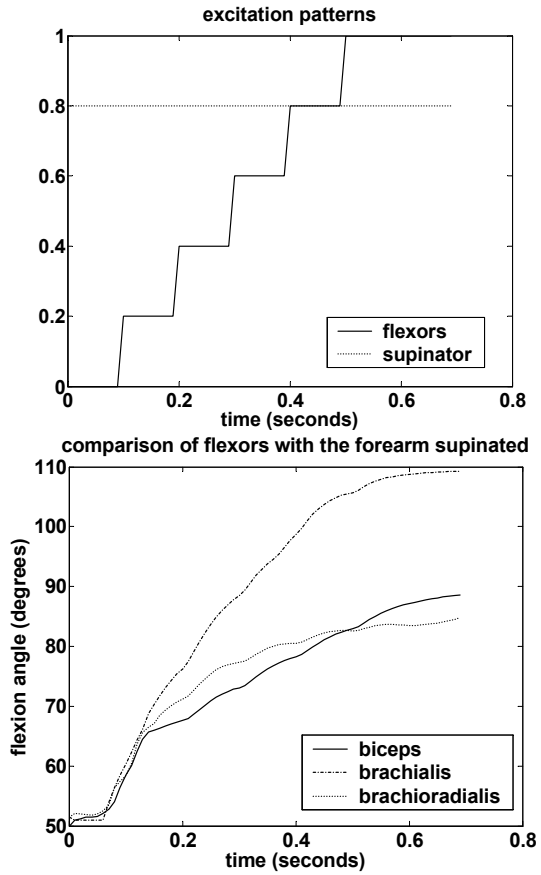

Figure 20. Effects of biceps (both heads), brachialis and brachioradialis on elbow flexion angle when the forearm is fully supinated.

Abduction of the humerus is achieved mainly through the action of the middle (lateral) deltoid. Indeed, activation of this muscle produced up to 78 degrees of abduction, contrary to the supraspinatus, which only reached 32 degrees. These results show that even full activation of the abductor muscles can only produce up to less than 90 degrees of abduction. The reason is that the humerus cannot be further elevated without accompanying scapular rotation. The upward scapular rotation provided by the upper and lower parts of the trapezius allowed the humerus to reach 121 degrees of abduction. This demonstrates how important the trapezius is for full abduction, and may indicate why it is not obtainable when this muscle is paralyzed.

The simulations reflected the importance of brachialis to flexion of the elbow, producing up to 109 degrees of flexion from any forearm position. Because the biceps also supinates as it flexes, it produces the most flexion from a supinated position. The brachioradialis inserts on the lateral side of the distal end of the radius and it usually participates in flexion when the movement is a fast one. This could not be seen since the dynamic properties of the muscles were not tested. However, it is also known that the brachioradialis is a particularly good flexor when the forearm is in a semiprone position (so that the thumb is up), and this was indeed demonstrated by the simulation results. For a variety of elbow flexor activation patterns, the supinator and the pronators (teres and quadratus) were able to maintain full supination and pronation of the forearm, respectively, with an excitation level of 0.8.

SIMM is a very powerful tool for musculoskeletal modeling since it allows easy manipulation of every element of the model through a graphical interface. New muscle elements can easily be added or removed, and their origins or insertions can be changed, e.g., to simulate a tendon transfer. In the same way, the maximum muscle force can be changed to represent individuals with spinal cord injury, and the range of motion of the various joints can be restrained to simulate other pathological conditions. The scapulothoracic gliding plane, which essentially makes the shoulder a closed-chain mechanism without being an actual joint, can be modeled in SIMM through the use of a constraint object. Also, the muscle lines of action can be adequately described by adding points and defining wrapping objects that represent bone surfaces. Finally, with the use of various tools for plotting, SIMM facilitates the analysis of movements and relations between forces and joint angles.

Since the shoulder is a complex mechanism, several simplifications were made to model it. Even for muscles with large attachment sites, the number of lines of action was no larger than twelve, which is important for computational reasons. However, it has been shown that the resulting error in the force capacity of the muscles in this approach is small [van der Helm and Veenbaas 1991]. Another simplification was the shape of the wrapping objects. These are supposed to represent bone surfaces, but currently only three shapes are available in SIMM: sphere, ellipsoid and cylinder. Since the bones do not have perfect shapes, the muscle lines of action cannot be precisely modeled, but these approximations probably have only minor impact on the results. The pronation-supination movement of the forearm was represented in this model as a rotation of the radius around an immobile ulna. However, this is not the way these two bones move relative to each other: Weinberg et al. (2001) demonstrated that the ulna performs an evasive motion during pronation and supination, but the effect of this small movement in the joint angles is probably insignificant. Similarly, the glenohumeral joint was modeled as a ball and socket joint, without translational degrees of freedom. In a study by Karduna et al (1996), it was shown that significant translation of the humeral head occurs with passive positioning of the joint, at the extremes of the range of motion. When the joints are positioned actively, muscle forces limit the translation, so the overall effect of this simplification is probably negligible.

The Hill model, the most commonly used muscle model in musculoskeletal modeling, makes certain assumptions that limit its accuracy in representing the dynamic properties of the muscles. Most Hill-type models assume that the dynamic parameters that contribute to force generation (i.e. activation, the force-velocity and the length-tension factors) are independent. Shue and Crago developed a Hill-type model that introduces length-dependent coupling between activation and velocity (Shue and Crago 1997). Another limitation of the Hill-type model is that it assumes that the static force-length relation also applies to dynamic simulations. It has been shown that there is a force depression following active shortening, which means that the isometric force produced after shortening is smaller than the pure isometric force produced at the corresponding length [Lee and Herzog, 2003]. This is not accounted for in the model. Finally, the current Hill-type model does not include the effect of history on muscle force: this could be degradation induced by fatigue, or enhancement induced by energy storage in the elastic elements of the muscle [Cavagna, 1997].

Besides its use in forward dynamic simulations, this model also has the potential to be used for inverse dynamic analyses. If a kinetics file is used as input, including the values of all the joint angles during a motion, the Dynamics Pipeline can calculate the joint torques required to generate that motion. However, it does not include optimization code to solve the load-sharing problem and calculate individual muscle forces. When this is added, the model can be used, for

example, to determine the muscles needed to be stimulated in order to restore specific functions in individuals with spinal cord injury.

Thorough validation of the model is not currently practical because the muscle excitation patterns that are the model inputs are not directly measurable in the actual musculoskeletal system. In most cases of tetraplegia, there will be certain muscles of the upper extremity under voluntary control and others that will be stimulated by the FES system. The input to the paralyzed muscles will be known theoretically because it will be determined by the FES controller, but it is infeasible to measure the neural input from the voluntary muscles; the problems in using EMG to approximate muscle excitation have already been discussed. Moreover, there are parameters used in the model, like the maximum muscle force, that cannot be directly measured in the real system and need to be approximated by values from cadaver studies or indirect joint moment measurements. This implies that the results of the model would not be in perfect agreement with the actual system even if measurement of the inputs was possible. For many applications, model simulations will be used to explore the effects of muscle sets included, to evaluate potential FES controllers, and to predict the outcome of various reconstructive surgeries. A perfect correspondence between the actual system and the simulated system is probably not required to reach general conclusions about such issues. A more rigorous validation of the model will eventually be achieved if and when the model-developed FES systems operate in the intended manner in human users.

References

Allinger, T.L. and Van den Bogert, A.J., (1997). “Skating technique for the straights, based on the optimization of a simulation model.” Occup Health Indust Med 36(6): 289.

Breteler, M.D.K., Spoor C.W. and Van der Helm, F.C.T., (1999). “Measuring muscle and joint geometry parameters of a shoulder for modeling purposes.” J Biomech 32:1191-97.

Cavagna, G.A. (1977). “Storage and utilization of elastic energy in skeletal muscle.” Exerc Sport Sci Rev 5:89-129.

Charlton, I.W. and Johnson, G.R., (2000). “An interactive musculoskeletal model of the upper limb.” Proc. ISG.

Cole, G.K., Van den Bogert, A.J., Herzog, W. and Gerritsen, G.M., (1996). “Modeling of force production in skeletal muscle undergoing stretch.” J Biomech 29(8): 1091-1104.

Creasy, G.H., Grill, J.H., Korsten, M., Sang, H., Betz, R., Anderson, R. and Walter, J., (2001). “An implantable neuroprosthesis for restoring bladder and bowel control to patients with spinal cord injuries: a multicenter trial.” Arch Phys Med Rehabil 82: 1512-19.

Davis, J.A., Triolo, R.J., Uhlir, J.P., Bhadra, N., Lissy, D.A., Nandurkar, S. and Marsolais, E.B., (2001). “Surgical technique for installing an eight-channel neuroprosthesis for standing.” Clin Ortho & Rel Res 385:237-252.

Dawodu, S.T., (2001). “Spinal cord injury: definition, epidemiology, pathophysiology.” eMedicine J 2(8).

Delp, S.L., (1995). “Computer modeling of movement abnormalities and their surgical corrections.” Gait & Posture 3(2):106.

Delp, S.L. and Loan, J.P. (1995). "A graphics-based software system to develop and analyze models of musculoskeletal structures." Comput Biol Med 25(1): 21-34.

DeLuca, C.J. and Forrest, W.J., (1973). “Force analysis of individual muscles acting simultaneously on the shoulder during isometric abduction.” J Biomech 6:385-393.

Dul, J.,(1987). “Shoulder muscle load during work with elevated arms.” Proc. 11th ISB –Congr., Biomech XI-A, pp.471-476, Free University Press, Amsterdam.

Happee R and Van der Helm, F.C., (1995). "The control of shoulder muscles during goal directed movements, an inverse dynamic analysis." J Biomech 28(10):1179-91.

Hogfors, C. Sigholm, G. and Herberts, P, (1987). "Biomechanical model of the human shoulder – I. Elements." J Biomech 20(2): 157-166.

Karduna A.R., Williams, G. R., Williams, J. L. and Iannotti, J. P., (1996): "Kinematics of the glenohumeral joint: influences of muscle forces, ligamentous constraints, and articular geometry." J Orhtop Res 14(6): 986-93.

Karlsson, D. and Peterson, B., (1992): "Towards a model for force predictions in the human shoulder." J Biomech 25(2): 189-199.

Keith, M.W., Peckham, P. H., Thrope, G. B., Buckett, J. R., Stroh, K. C. and Menger, V. (1988). "Funcional neuromuscular stimulation neuroprostheses for the tetraplegic hand." Clin Orthop 233:25-33.

Keith, M.W. and Lacey, E.H., (1991). "Surgical rehabilitation of the tetraplegic upper extremity." J Neuro Rehab 5:75-87.

Lee, HD and Herzog, W., (2003). "Force depression following muscle shortening of voluntarily activated and electrically stimulated human adductor pollicis." J Physiol , June18th.

Lemay, M.A. and Crago, P.E., (1996). "A dynamic model for simulating movements of the elbow, forearm and wrist." J Biomech 29(10): 1319-30.

Nigg, B.M. and Herzog, W., (1999). "Biomechanics of the musculoskeletal system." University of Calgary, Calgary, Alberta, Canada, John Wiley & Sons.

Parikh, P.P. Acosta, A.A. and Kirsch, R.F., (2003). "Voluntary synergistic control of shoulder muscle FNS patterns in C5 tetraplegia." *Not yet published*.

Poppen, N.K. and Walker, P.S., (1978). "Forces at the glenohumeral joint in abduction." Clin Orthop Rel Res 135:165-170.

Praagman M., Veeger, H.E.J., Chadwick, E.K.J., Colier, W.N.J.M. and Van der Helm, F.C.T., (2003). "Muscle oxygen consumption, determined by NIRS, in relation to external force and EMG." J Biomech 36: 905-912.

Shue, G.H. and Crago, P.E., (1997). "Muscle-tendon model with length history-dependent activation-velocity coupling." Annals of Biomed Eng 26: 369-380).

Van den Bogert, A.J., Gerritsen, K.G.M. and Cole, G.K., (1998). "Human muscle modeling from a user's perspective." J Electr Kines 8: 119-124.

Stolov, W. and Clowers, M.,(Eds.) (1981). "Handbook of Severe Disability". Washington, D.C.: U.S. Government Printing Office.

Van der Helm, F.C.T. and Veenbaas,R., (1991). "Modeling the mechanical effect of muscles with large attachment sites: application to the shoulder mechanism." J Biomech 24(12): 1151-63.

Van der Helm, F. C., Veeger, H.E.J., Pronk, G.M., Van der Woude, L.H.V. and Rozendal R.H., (1992). "Geometry parameters for musculoskeletal modelling of the shoulder system." J Biomech 25(2): 129-44.

Van der Helm, F.C.T, (1994): "A finite element musculoskeletal model of the shoulder mechanism." J Biomech 27(5): 551-569.

Van der Helm, F.C.T. and Chadwick, E.K.J., (2003). "A forward-dynamic shoulder and elbow model." *Not yet published*.

Veeger, H. E., Van der Helm, F.C.T., Van der Woude, L.H.V., Pronk, G.M. and Rozendal, R.H., (1991). "Inertia and muscle contraction parameters for musculoskeletal modelling of the shoulder mechanism." J Biomech 24(7): 615-29.

Veeger, H. E., Yu, B., An, K.N. and Rozendal H., (1997). "Parameters for modeling the upper extremity." J Biomech 30(6): 647-52.

Van Soest, A.J., Schwab, A.L., Bobbert, M.F. and Van Ingen Schenau, G.J., (1992). "SPACAR: a software subroutine package for simulation of the behavior of biomechanical systems." J Biomech 25(10): 1219-26.

Weinberg, A.M., Pietsch, I. T., Krefft, M., Pape, H. C., van Griensven, M., Helm, M. B., Reilmann, H. and Tscherne, H. (2001). "Pronation and supination of the forearm. With special reference to the humero-ulnar articulation." Unfallchirurg 104(5): 404-9.

Winters, J.M. and L. Stark, L., (1985). "Analysis of fundamental human movement patterns through the use of in-depth antagonistic muscle models." IEEE Trans Biomed Eng 32(10): 826-839.

Wood, J.E., Meek S.G. and Jacobsen S.C., (1989). "Quantitation of human shoulder anatomy for prosthetic arm control – I. Surface modeling." J Biomech 22(3): 273-292.

Yamaguchi, G.T. and Zajac, F.E., (1990). "Restoring unassisted natural gait to paraplegics via functional neuromuscular stimulation: a computer simulation study." IEEE Trans Biomed Eng 37(9): 886-902.

Zahalak, G.I, (1986). "A comparison of the mechanical behavior of the cat soleus muscle with a distribution-moment model." J Biomech Eng 108:131-140.

Zajac, F.E, (1993). "Muscle coordination of movement: a perspective." J. Biomech 26 Supp.1: 109-124.

Appendix A: The standardized shoulder protocol[1]

Global co-ordinate system:
X_g: horizontal, pointing from left to right.
Y_g: vertical, pointing upward.
Z_g: horizontal, pointing backward.

Thorax
$^{G}y_t$: $\frac{\{(^{\prime}\underline{IJ}+^{\prime}\underline{C7})/2-(^{\prime}\underline{PX}+^{\prime}\underline{T8})/2\}}{\|(^{\prime}\underline{IJ}+^{\prime}\underline{C7})/2-(^{\prime}\underline{PX}+^{\prime}\underline{T8})/2\|}$
(vector from the midpoint between PX and T8 to the midpoint between IJ and C7, approximately vertical in the initial position)
$^{G}x_t$: Perpendicular to the plane fitted to the points ^{G}IJ, ^{G}C7 and (^{G}PX + ^{G}T8)/2, pointing to the right.
$^{G}z_t$: Perpendicular to $^{G}x_t$ and $^{G}y_t$.
Origin: ^{G}IJ (incisura jugularis)

Clavicle
$^{G}x_c$: $(^{G}\underline{AC} - {}^{G}\underline{SC}) / \|(^{G}\underline{AC} - {}^{G}\underline{SC})\|$
$^{G}z_c$: Perpendicular to $^{G}x_c$ and $^{G}y_t$, pointing backward.
$^{G}y_c$: Perpendicular to $^{G}z_c$ and $^{G}x_c$.
Origin: ^{G}SC

Scapula
$^{G}x_s$: (^{G}AA - ^{G}TS) / |(^{G}AA - ^{G}TS) |
$^{G}z_s$: Perpendicular to (^{G}AI - ^{G}AA) and $^{G}x_s$, pointing backward, i.e. perpendicular to the scapular plane.
$^{G}y_s$: Perpendicular to $^{G}z_s$ and $^{G}x_s$.
Origin: ^{G}AA

Humerus
$^{G}y_h$: $(^{G}\underline{GH} - {}^{G}\underline{E}) / \|(^{G}\underline{GH} - {}^{G}\underline{E})\|$.
$^{G}z_h$: Perpendicular to $^{G}y_h$ and (^{G}EL - ^{G}EM), pointing backward.
$^{G}x_h$: Perpendicular to $^{G}y_h$ and $^{G}z_h$.
Origin: ^{G}GH

[1] from: "A standardized protocol for motion recordings of the shoulder", Frans CT van der Helm, Department of Mechanical Engineering and Marine Technology, Technische Universiteit Delft, The Netherlands

The degrees of freedom of the model are also obtained from the shoulder protocol:

Joint	*Degrees of freedom*	*Description*
Sternoclavicular	SC y	Protraction/retraction about the thoracic y axis
	SC z'	Elevation/depression about the local z axis
	SC x''	Axial rotation about the local x axis
Acromioclavicular	AC y	Protraction/retraction about the clavicular y axis
	AC z'	Lateral/medial rotation about the local z axis
	AC x''	Tipping forward/backward about the local x axis
Glenohumeral	GH y	Plane of elevation with respect to the scapular y axis
	GH z'	Elevation/depression about the local z axis
	GH y''	Axial rotation about the local y axis
Humero-ulnar	EL x	Elbow flexion/extension
Ulno-radial	PS y	Forearm pronation/supination

Appendix B

Muscle	*Number of elements*
Trapezius, scapular part (middle and lower)	11
Trapezius, clavivular part (upper)	2
Levator scapulae	2
Pectoralis minor	4
Rhomboid	5
Serratus anterior	12
Deltoid, scapular part (posterior and middle)	11
Deltoid, clavicular part (anterior)	4
Coracobrachialis	3
Infraspinatus	6
Teres minor	3
Teres major	4
Supraspinatus	4
Subscapularis	11
Biceps, long head	1
Biceps, short head	2
Triceps, long head	4
Triceps, medial head	5
Triceps, lateral head	5
Latissimus dorsi	6
Pectoralis major, thoracic part	6
Pectoralis major, clavicular part	2
Brachialis	7
Brachioradialis	3
Pronator teres	2
Supinator	5
Pronator quadratus	3
Anconeus	5

A Robotic Facility for Evaluation of Control Sources to Restore Arm Function via FNS to Individuals with High Level Tetraplegia

Contract section: E.1.a.iv Command sources for high tetraplegia

Abstract

The purpose of this project is to develop a robot system to emulate the kinematics and dynamics of a human arm, so that it enables faster evaluations of a larger number of candidate controllers of an advanced neuroprosthetic system.

Methods and Results

In order to simulate the behavior of a paralyzed arm, a six degree-of-freedom revolute robot has been purchased and installed in an inverted position (Figure 21). The model acquired is a Staubli RX60. This specific model was selected for its relative size to a human arm. The master controller of the system will be provided by a PC running the xPC Target software (The Mathworks, Inc.).

The mounting of the robot was designed such that deflections due to motion of the robot were below 0.254 mm at the end of the arm. The maximum moments specified by the manufacturer were used as the disturbances to the column. Qualitative assessment of the structure indicates that it is stiff enough to resist the loads that will be placed upon it. The arm itself is mounted at a height that approximates the height of a human shoulder while seated.

The RX60 robot is one of the smallest articulating arms on the market. It has a reach of 660 mm, comparable to an average human reach of 650 mm. The maximum payload is 4 kg at low speed at 2 kg at full speed. This capacity is sufficient when compared to the strength of individuals with spinal cord injury using an FES device. The size of the arm was kept close to that of a human's in order to both interact with a typical work environment as well as provide a

(a) (b)

Figure 21. Photographs of robot arm mounting in starting position (a) and a typical application position. A meter stick is shown as a reference.

better sense of applicability in the eye of the operator.

The robot is controlled by a Staubli CS8 controller for precise joint positioning. Position commands can be carried out using either specific joint angles or end point positions. The amount of smoothing between positions (leave) can be adjusted but will most likely be set to zero as a stimulated paralyzed arm does not have any such control. Joint positions will be sent to the CS8 through a serial interface with an external Master Controller (MC). The CS8 has 16 I/O ports available for additional information transfer if necessary.

The overall master controller of the system is an embedded PC running the Mathworks' xPC Target operating system. This controller will operate as an interface between the commands from the operator and the joint position controller of the robot (Figure 22). Initially it will convert the commands into accurate joint positions. Later, the joint positions to the robot will be "corrupted" to simulate the behavior of a stimulated paralyzed arm. Corrupting information will include random position and velocity errors as well as weakness in some directions of motion. Command sources will be input to the master controller through either a serial interface, analog or digital input.

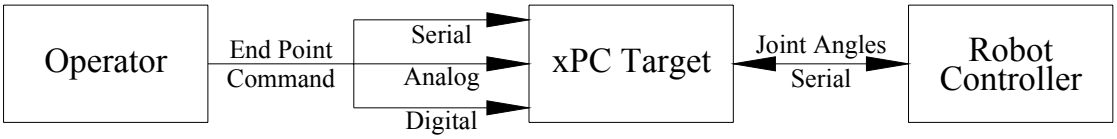

Figure 22. Information flow.

An error checking serial interface has been developed to communicate between the MC and the CS8. The interface operates in binary mode at 115,200 baud using 8N1 serial protocol. Joint angles are sent as two bytes each (12 total) between 0 and 255 and reconstructed on the robot side into decimal values between -90 and 90 with $.02^{o}$ resolution. To align the information streaming from the MC, a synchronize byte as well as a checksum byte are also passed to the robot. In the event of a dropped byte (receive error), the system interpolates the next point based upon its previous direction of motion and corrects itself on the next iteration of the program loop. A final byte is sent as a command to either open or close the end of the arm tooling. Actual joints angles can also be sent back to the MC to provide further error checking. This feature will be used primarily in quantitative tests of command source information transfer rate. Commands are issued to the robot at 10 Hz and the robot movement buffer is cleared every seven iterations of the program loop to provide smooth arm motion.

A pneumatic end-effector (Figure 23a) has been built to grasp large cups such as thermal insulated coffee mugs (~70mm diameter, Figure 23b). The choice of grasping relatively large objects was made for simplicity purposes, and is a first step toward manipulating smaller objects. Additional fingers can easily be fabricated for the generic pneumatic actuator, depending on the size of objects to be picked up. The actuator is an SMC double-acting pneumatic gripper with a 30^{o} range of motion.

(a)

(b)

Figure 23. Photographs of the end of arm tooling (a) and the cup it was designed to manipulate (b).

A qualitative test of the system has been performed where an operator uses both head orientation and facial EMG as command sources to the MC. A three-axis orientation sensor (MicroStrain 3DM) communicating via a serial interface at 50Hz was used to command gripper position within a plane centered at the shoulder. Facial EMG from the frontalis muscle was used as a state command for the gripper. The EMG was sampled at 100 Hz, and a spike crossing over a preset threshold indicated a state change. Two routines were tested, one where the user's state command only opened or closed the gripper and another that triggered a sub-routine which brought the grasped object to a position in front of the user's face. In the case of the second routine, the object was returned to its previous position on the table following a second state change. Using this second method, the user was able to simulate drinking from the cup (using a straw) with command sources located on the head as sole inputs to the robot arm.

Forward and inverse kinematics for the robot arm have been developed such that conversions between room space and joint space can be performed. Room space coordinates include Cartesian, cylindrical, and spherical reference frames. This allows for user commands in one of three coordinates (depending on user comfort) to be translated into joint angle commands to the robot, as well as joint information from the robot to be converted back for evaluation purposes. This interplay between room and joint spaces will be used extensively in quantitative assessment of command source information transfer rate, comparing instructed and actual end point positions.

Next quarter

The communications interface between human subjects and the robotic arm will be finalized over the next 2 months. Testing of several candidate command sources, such as voice commands, head movements, and eye movements, will then begin.

Supplemental Feedback to Enhance Myoelectric Control in a Neuroprosthesis

Contract section: E.1.a.v Sensory feedback of contact and grasp force

Note: The following is the abstract from a masters thesis. The full document is available upon request (Kumar, Charisma; "Supplemental Feedback to Enhance Myoelectric Control in a Neuroprosthesis", M.S. Thesis, Dept. of Biomed. Eng., CWRU, May 2003).

Abstract

A new development in the hand neuroprosthesis uses myoelectric signals from volitional wrist muscles as a control signal. Neuroprosthetic users have a loss of sensation below the level of their spinal cord injury. Supplemental myoelectric feedback may augment the ability to control their prosthesis.

A supplemental feedback system using auditory stimuli was implemented to assist subjects in myoelectric control of a simulated hand. An experimental paradigm was designed to compare subjects' ability to maintain myoelectric control while performing certain tasks.

Six able-bodied subjects evaluated the effects of supplemental feedback in maintaining hand position in the absence of visual feedback. The tasks performed resembled drinking, eating and lifting an object. The two feedback conditions being compared were the presence and absence of auditory cues. Analysis of variance and success rates were used as indicators of performance. We found that supplemental myoelectric feedback significantly improved the subject's ability to maintain control.

Wireless Data Acquisition Module for Use with a Neuroprosthesis

Contract section*:* E.1.a.v Sensory feedback of contact and grasp force

Abstract

A general wireless data acquisition module (WDAM) is being developed for use with a neuroprosthesis. The WDAM is intended to be used with sensors such as the shoulder or wrist position transducer, finger-mounted joysticks, or remote on-off switches. Currently these sensors are connected to a controller via cables, which are cosmetically unappealing to the user and often get caught on wheelchairs, causing them to be damaged. Switch-activated transmitters mounted on walkers have been used previously in FES applications [1]. Recent advances in wireless technology have reduced the complexity and size of the wireless circuitry and have increased the likelihood that a small, low power, reliable wireless link could be assembled from commercially available components.

Methods

Prototype circuit

In a previous progress report, successful data transmission from one transceiver module to another (including error-checking and acknowledgement) was described. These tests were performed using a combination of the microprocessor development kit from Microchip, Inc. and

the transceiver development kit from RF Monolithics. These development kits contained extra circuit components (e.g., LEDs, potentiometers) that are not needed for our application. A prototype circuit was built to demonstrate more accurately the size and power requirements for the wireless data acquisition module. A block diagram of the circuit components is shown in Figure 24.

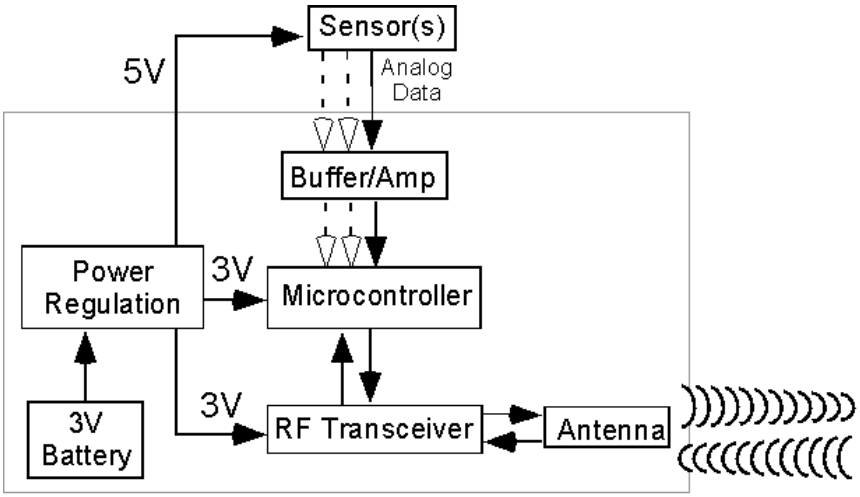

Figure 24. Block diagram of wireless data acquisition module circuit.

Besides the microcontroller and transceiver, the prototype circuit includes a power regulation section that uses DC-DC converters to provide stable 5 volt power to the sensors and stable 3 volt power to the rest of the circuit. In addition a buffer/amplifier section was included between the sensors and the microcontroller to limit the analog input range to 3 volts.

Battery options

For testing purposes, two AA batteries were used to power the prototype circuit. Since the desired size for the WDAM is approximately a 1 inch cube, a review of available button or coin cell batteries was made. Both primary (one-use) and secondary (rechargeable) batteries were examined. Variables such as battery chemistry, size, voltage, capacity and maximum discharge current were considered.

Results

Prototype circuit

The development kits that were tested in a previous progress report used 25.7 – 32.1 mA during data transmission. The prototype circuit described above uses 4.1 - 5.2 mA (without any sensors attached). A single-axis accelerometer connected to the circuit required another 16 mA.

The successful data transmission rate with the development kits had been 100%. This rate has dropped to 94% with the new prototype circuit. It is believed that the reduced rate is due to noise that is being picked up by the point-to-point wiring in the prototype circuit. A planned printed circuit board version should reduce the amount of noise.

Battery options

The selection of a battery requires a series of compromises involving cell size, battery chemistry, capacity, maximum discharge current, and voltage. Due to the size constraints of the WDAM, a button or coin cell battery configuration is desirable. There are a variety of battery chemistry choices for primary (one-time use) cells and secondary (rechargeable) cells. The advantages and disadvantages are shown in Table 3.

Battery Type	Advantages	Disadvantages
Primary	Higher capacities	Need to be replaced by user
Lithium	3 V, lightweight	Low discharge current
Silver Oxide	High energy density	1.5 V (need 2)
Zinc Air	Highest energy density	1.4 V (need 2), needs air flow
Secondary	Package can be sealed	Lower capacity, need recharge method
Lithium-ion	3 V, lightweight	Recharge safety issues, availability, more expensive
NiMH	Higher energy density than NiCd	1.2 V (need 2-3), reduced cycle life for digital loads

Table 3. Battery type advantages and disadvantages.

The current plan is to initially utilize a primary battery system that the user can replace. Subsequent versions will incorporate a rechargeable battery if the capacity and discharge current requirements can be met. A lithium primary battery will be selected once the current requirements of the WDAM are further reduced in the next quarter.

Next quarter

In the next quarter, three methods of reducing the current requirements further will be investigated:

1. Add master/slave routines. Presently, the sampled data is transmitted continuously as fast as possible. Since transmitting data requires more power than receiving, the current needed can be reduced by having the sensor module in 'slave' mode, waiting for a request for data from the 'master' module.

2. Utilize sleep functions. Presently, the microprocessor and transceiver are powered continuously. Once the master/slave routines above are set up, the 'slave' module can be put in sleep mode (which requires much less power) until a data request is received.

3. Utilize faster transceiver modules. Presently, the transceiver module is designed to support a data transmission rate of 19.2 kbps. RF Monolithics has recently come out with newer versions that support data transmission rates of 115.2 kbps and 1 Mbps. Although we do not anticipate needing continuous data

transmission rates that are that high, the quicker rates will allow the transceiver to spend more time in sleep mode. These newer modules have been ordered.

References

[1] Z. Matjacic, M. Munih, T. Bajd, A. Kralj, H. Benko, and P. Obreza, "Wireless control of functional electrical stimulation systems," *Artif Organs*, vol. 21, pp. 197-200, 1997.

Percutaneous Implementation of Myoelectric Controlled Neuroprosthesis: A Case Study

Contract section: E.1.b Control of Grasp Release in Lower Level Tetraplegia

Abstract

The purpose of this research is to develop and evaluate an advanced neuroprosthesis (NP) to restore hand function in persons with low cervical spinal cord injuries. Through this work we will implement in human subjects a control methodology utilizing myoelectric signals (MES) from muscles that can act in synergy with hand function to govern the activation of paralyzed, electrically stimulatable muscles of the forearm and hand. This work encompasses the following objectives:

1) Characterize the MES recorded from a pair of muscles synergistic to hand function, demonstrating that the signals are suitable for NP control.
2) Demonstrate the ability of subjects to use the proposed control algorithm to perform simulated NP functions and to control a virtual hand.
3) Implement myoelectric control of the hand grasp NP in subjects with low cervical spinal cord injury and evaluate hand performance.

Progress Report

Previous studies demonstrated that MES patterns from wrist flexor and extensor muscles were adequately distinct to enable reliable NP state selection and command modulation when no stimulation was applied to the hand. During this quarter, a percutaneous NP was implemented in a subject with tetraplegia secondary to spinal cord injury at C6/7. The system included 12 electrodes for muscle stimulation and 2 electrodes for recording MES for control from the wrist flexor and extensor muscles. The objectives of the study were to demonstrate the effective elimination of stimulation artifact and evaluate and compare the controllability, impairment, and function of the hand when the NP was controlled with MES and with an external wrist position sensor.

Subject and Electrode Implantation

The subject was a 36-year old male who sustained a spinal cord injury 2 years and 9 months prior to the study. His neurological classification was C6 ASIA complete bilaterally. He was Group 4 by the International Classification on the right side, and Group 3 on the left. He had grade 4+ wrist extension and 3- wrist flexion on his right side, which was implemented with the NP. He also retained weak voluntary finger and thumb flexion and extension which, with

tenodesis action accompanying wrist extension, gave him a functional pinch that allowed him to perform most self-care activities independently. He was interested in knowing whether an FES system would increase his grasp strength and improve his hand function.

Percutaneous intramuscular electrodes for muscle stimulation and MES recording were implanted in an outpatient clinical procedure. The stimulation electrodes and the implantation procedure have been described elsewhere [1,2]. The electrodes were implanted so that their insertion sites were localized to two areas of skin, one on the dorsal aspect of the forearm and the other on the volar aspect. Electrodes were implanted in the thumb abductor, adductor, extensor, and flexor muscles and in the finger flexors and extensors, both intrinsic and extrinsic. The MES electrodes consisted of a pair of insulated stainless steel wires wound into a coiled lead [3] (Figure 25). Both wires were de-insulated at their ends and the second wire was wound over the first, forming an electrode with two 2 mm de-insulated sections separated by 4 mm. MES electrodes were implanted in the extensor carpi radialis brevis (ECRB) and flexor carpi radialis (FCR). The electrode wires exiting the skin were trimmed and crimped to connectors used for interfacing with stimulation and recording equipment.

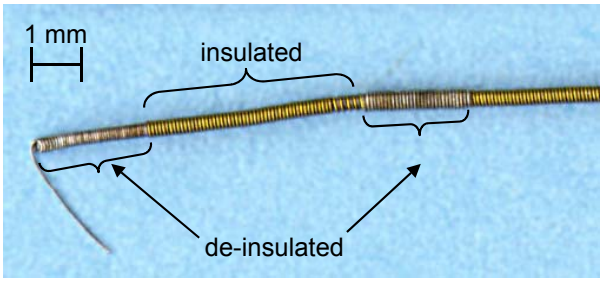

Figure 25. Percutaneous bifilar MES recording electrode [3].

Experiments were performed as an outpatient. All procedures received IRB approval and informed consent was obtained.

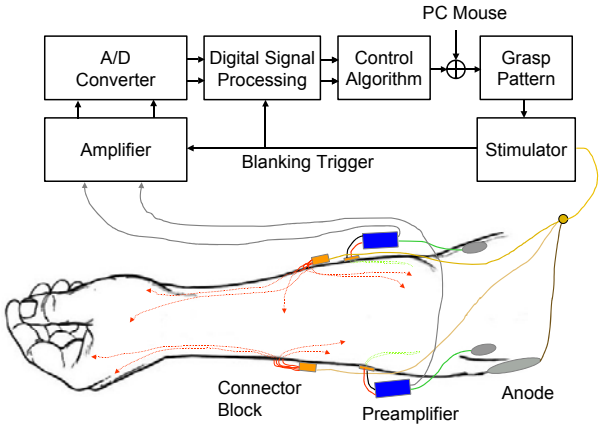

Figure 26. Block diagram of experimental setup.

Instrumentation

The MES-controlled percutaneous NP consisted of electrodes, MES preamplifiers, a blanking amplifier, a computer, and a stimulator (Figure 26). The blanking amplifier (Cambridge Electronic Design, Ltd.) grounded the MES inputs, essentially zeroing the MES, for a programmed duration in response to a trigger signal. The trigger signal was a single pulse received from the stimulator at the beginning of every stimulus period. The computer smoothed the digitized MES using a rectified averaging technique and fed the artifact-free, processed MES to a control algorithm. The control algorithm calculated a command signal based on the MES recorded from the wrist muscles. Alternatively, the command signal could be modulated using the computer mouse. The grasp pattern mapped the command level to stimulus parameters for each stimulation electrode so that command signal modulation resulted in coordinated stimulation of hand opening and closing in a functional pattern. The grasp pattern and control algorithm were customized to the subject.

Stimulated Grasp Patterns

Lateral and palmar grasp patterns were programmed into the stimulator [4]. Eleven electrodes were used in the lateral grasp, and ten were used in the palmar grasp. Muscle recruitment was achieved by pulse-width modulation. The stimulus pulses were delivered at a rate of 12 Hz (83 msec stimulus period) in both grasp patterns. The maximum time difference between the first and last pulse delivered every stimulus period was 24 msec in the lateral grasp and 22 msec in the palmar grasp.

Percutaneous stimulation enabled the development of both grasp patterns and brought the thumb and fingers into correct opposition for grasping. However, the absence of a strong stimulated index finger flexor and thumb adductor limited the amount of lateral pinch strength that could be added to the voluntary pinch. This is an effect of using percutaneous electrodes, and generally is not experienced with implanted systems. In the palmar pinch, clawing of the fingers occurred with stimulation at 0% command (full finger extension), and worsened when the forearm was held in a prone position, a condition that could not be completely eliminated by adjusting the stimulation. The stimulation pulse amplitudes were fixed at 20 mA on all but two electrodes; one FDS electrode was set to 8 mA, and the EDC electrode was set to 2 mA. Graded recruitment of the EDC was not possible even with the low current amplitude, resulting in quite abrupt finger extension.

Stimulus Artifact Suppression

With the wrist muscles relaxed, MES were recorded as the command level was manually ranged. The stimulus artifact was observed in the MES and the blanking amplifier was programmed to zero the MES for a duration that was determined by examining the duration of stimulation artifact. The trial was repeated with artifact suppression activated to assess the effectiveness of the artifact suppression technique.

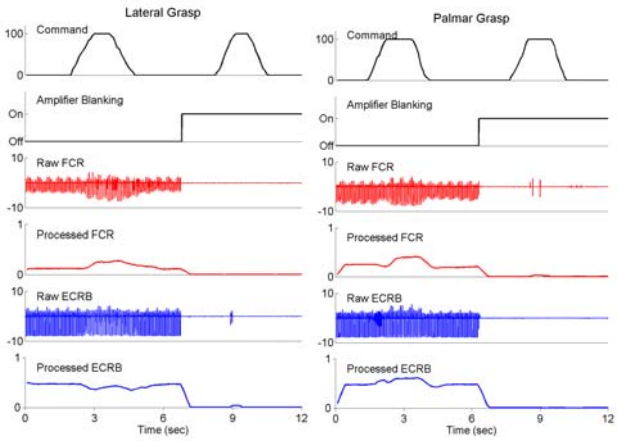

Figure 27. Stimulation artifact suppression during both grasp patterns while muscles were

The duration and amplitude of the total stimulation artifact created in a stimulus period varied with command level, grasp pattern, and muscle from which MES was recorded (Figure 27). A blanking duration of 42 msec at the beginning of every stimulus period was found to adequately suppress stimulation artifact.

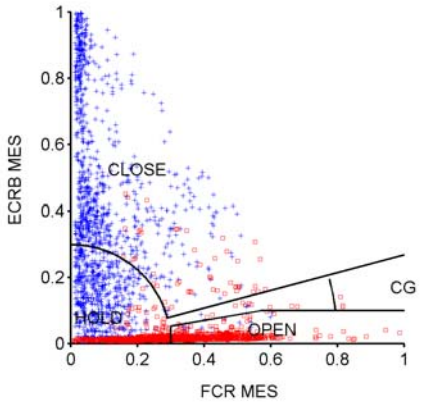

Figure 28. MES data during sustained wrist flexion (□) and extension (+) with and without stimulation on. Boundaries defined the NP states.

Control Algorithm Customization

MES were recorded during sustained wrist flexion, extension, and rest while the muscles of the hand and forearm were being stimulated at various command levels and with the arm and forearm held in different

static arm and forearm postures (see QPR #5). Wrist flexion and extension data are shown in Figure 28. This figure shows the processed myoelectric activity from the FCR and the ECRB over all of the experimental trials. The solid lines show baseline thresholds and boundaries, which partitioned the signal space into NP states. More co-contraction occurred during wrist extension than during wrist flexion. The thresholds were determined by inspection and were placed so that they enclosed at least 90% of the data. The thresholds and boundaries were incorporated into the myoelectric control algorithm, which calculated the NP state (Open, Close, Hold, or Change Grasp) and command level based on the instantaneous MES recorded in the ECRB and FCR.

Neuroprosthesis Control

The position matching test (described in QPR#6) was conducted to compare the subject's ability to modulate the command signal using myoelectric control and wrist position control. An external electrogoniometer (Penny & Giles) was used to record wrist position, which when using wrist position control was linearly mapped to the command signal over the range of -30° to 30°. The test required the subject to control the opening and closing of the needles of an on-screen dial (simulated hand), and attempt to match within +/- 5% target positions superimposed on the dial. An error was registered whenever the subject-controlled hand position moved away from the target position. The test was conducted with no stimulation on, with lateral grasp stimulation, and with palmar grasp stimulation, and with the forearm held in a neutral and prone

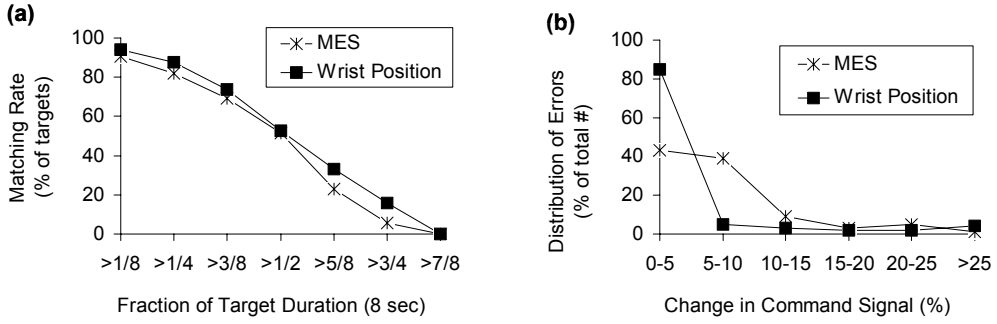

Figure 29. Neuroprosthesis control. The results from all six position matching test trials were pooled for both control method. (a) Matching Rate, the percentage of 180 targets presented that were matched for specified fractions of the total target duration. (b) Distribution of Errors, the percentage of the total number of errors for specified magnitudes of inadvertent command change they caused.

posture. These conditions resulted in six trials for each control method.

The subject was able to use both MES and wrist position control to modulate the command level (position of simulated hand) and maintain it at desired levels in the Position Matching Test. The percentage of target command levels matched for at least 2 consecutive seconds was 82% using MES control and 88% using wrist position control (Figure 29(a)). The magnitude of inadvertent change in command was usually small. When using MES control, 43% of the errors caused command changes of less than 5%, and 91% of the errors caused command changes of less than 15% (Figure 29(b)). When using wrist position control, 85% of the errors caused command changes of less than 5%, and 92% of the errors caused command changes of less than 15%. With MES control, the size of inadvertent command change was also directly

related to the speed of command modulation, which in these tests was directly proportional to the magnitude of the MES, but limited to speeds between 25% per second and 100% per second. These results are within the range of those obtained in previous experiments of MES control when no stimulation was used.

Pinch Force and Grasp Release Test

Palmar and lateral pinch force with and without the NP was measured with a pinch meter (Figure 30). Although stimulating at 100% command (full hand closure with full force), the lateral pinch force was not significantly different from that produced without electrical stimulation ($p = 0.69$, Wilcoxon rank sum test). However, a statistically significant difference in palmar pinch force was found ($p=0.02$), where the force measured with the NP was less than that produced without it. It is not clear why the pinch force did not improve with stimulation, or at least remain as strong as it was without the stimulation. Our subject affirmed that he was exerting the same amount of effort during all the measurements. The stimulation might have prevented the fingers and thumb from making optimally-oriented contact with the pinch meter, thereby misdirecting the pinch force, resulting in a lower measurement.

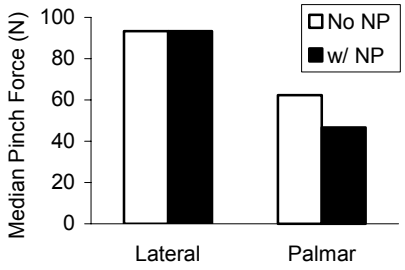

Figure 30. Pinch force with and without the NP for lateral and palmar grasp.

The Grasp Release Test (GRT) [5] was conducted without the NP, with the NP controlled by MES, and with the NP controlled by wrist position. Three standard GRT objects – the peg, block, and paperweight, and three larger and heavier objects than standard – a can, book, and squeeze bottle, were used in the test. The heavier objects were included because it was anticipated that differences in performance with and without the NP would be more apparent. The test required the subject to grasp an object, lift it over a barrier, and release the object in a target area as many times as possible within 30 seconds. The number of successful task completions was counted. A 30-second trial was run three times for each object.

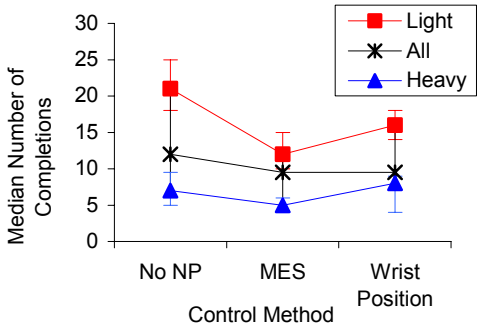

Figure 31. Grasp Release Test comparison of two NP control methods. Median number (and interquartile range) of task completions in 30 seconds. Light objects (peg, block, paperweight); heavy objects (can, book, bottle).

The subject's performance on the GRT did not change significantly with respect to the NP control method (MES vs. wrist position) when the total number of task completions across all the objects were compared ($p=0.40$, Wilcoxon rank sum test) (Figure 31). His performance without the NP was as good or better than it was with the NP regardless of control method. He performed better ($p<0.001$, No NP vs. MES; $p=0.02$, No NP vs. wrist position) without the NP when handling the light objects, but there was no significant difference in performance with or without the NP ($p=0.11$, No NP vs. MES; $p=0.48$, No NP vs. wrist position) when handling the heavy objects. Handling the light objects did not require much wrist action, therefore adequate MES was not produced to appropriately modulate the command signal. Instead, the command level remained fairly constant during most

of the trial and the stimulation did not provide hand movement that was in synchrony with the subject's voluntary function. With the heavy objects, adequate MES was produced, the command signal was appropriately modulated, and stimulation was delivered in synchrony with the desired hand function. Potential reasons why the percutaneous stimulation did not supplement voluntary function in the heavy object tasks include unconditioned muscles, misdirected force application to the objects, electrode placement, or muscle recruitment properties.

Functional Activities

The subject was video-taped while performing several functional activities with and without the NP controlled by MES. The activities included unscrewing a bottle cap, pouring from a bottle, picking up and releasing a cup, and pulling a 35-lb box with a rope. The subject was able to perform all of the activities with and without the NP, except one. He was unable to pull the 35-lb box without the NP, and was only able to budge it slightly with the stimulated lateral grasp before the grip slipped. While it was clear to both the investigator and participant that the stimulation did improve his voluntary pinch strength during the pulling task, the NP seemed to make it more difficult for the subject to unscrew the bottle cap and acquire the cup. Unscrewing the bottle cap required the subject to hold the bottle between his knees and repeatedly pinch the cap between the index finger and thumb and twist until the cap came off. Without the NP, the subject was able to repeatedly loosen and tighten his thumb's grip on the cap with little wrist motion, which allowed him to perform the task easily. With the NP, he had difficulty opening his thumb to reposition it once it was fully closed, because it was not advantageous for him to flex his wrist while trying to grip the bottle cap. In acquiring the cup without the NP, the subject was able to lower his hand upon and wrap around the cup. With the NP, he had to flex the wrist significantly and wait for the hand to fully open before bringing it to the cup.

Conclusions

Stimulation artifact created in wrist muscles by intramuscular stimulation of forearm and hand muscles was effectively suppressed, allowing the MES to be used for control of a hand grasp neuroprosthesis. The myoelectric control strategy enabled the subject to open and close his hand by activating NP states and modulating the command signal with good reliability. However, the myoelectric control strategy appeared to be limited in its utility during hand grasp tasks that required rapid opening and closing of the hand, or frequent adjustments of the grip. Unless the object to be handled was heavy, or the task required much wrist action, MES of adequate magnitude was not produced and the stimulation did not augment hand function, but may have actually hampered hand function. The myoelectric control strategy was better suited to tasks that required the subject to maintain a constant grip for an extended period of time. The subject has a very functional voluntary grasp that allowed him to achieve a GRT score without the NP that was much higher than the average GRT scores reported from 38 individuals with C6 SCI [6]. The GRT score was not improved with the percutaneous NP. Improving grasp function in such an individual is a great challenge. The control strategy may be appropriate for individuals with greater hand impairment than the subject studied. The wrist position control strategy did not prove to be statistically different than MES control, but it felt more responsive to the subject. It also did not require as much wrist motion to produce full command modulation. A myoelectric control strategy in which the command signal is made proportional to the

difference in FCR and ECRB MES may mimic a wrist position controller and provide the user a greater sense of control and enable quick hand manipulations and grip adjustments. Additional studies will be performed to investigate this possibility.

Next Quarter

We will continue investigating the practical utility of the myoelectric control strategy in subjects with low cervical SCI. Additional myoelectric control strategies will be tested, particularly one in which the command signal is made directly proportional to the MES or MES difference.

References

[1] Peckham, P.H.; Marsolais, E.B.; Mortimer, J.T. "Restoration of key grip and release in the C6 tetraplegic patient through functional electrical stimulation," *J. Hand Surg.,* **5A** (1980) 462-469.

[2] Knutson, J.S.; Naples, G.G.; Peckham, P.H.; Keith, M.W. "Electrode fracture rates and occurrences of infection and granuloma associated with percutaneous intramuscular electrodes in upper-limb functional electrical stimulation applications," *J. Rehabil. Res. Dev.,* **39** (2002) 671-684.

[3] Mortimer, J.T.; Yodlowski, E.H. "Frequency sweep analysis of neuromuscular junction continuity," *J. Med. Eng. Technol.,* **3** (1979) 242-247.

[4] Kilgore, K.L.;. Peckham, P.H.; Thrope, G.B.; Keith, M.W.; Gallaher-Stone, K.A. "Synthesis of hand grasp using functional neuromuscular stimulation," *IEEE Trans. Biomed. Eng.*, **36** (1989) 761-770.

[5] Wuolle, K.S.; VanDoren, C.L.; Thrope, G.B.; Keith, M.W.; Peckham, P.H. "Development of a quantitative hand grasp and release test for patients with tetraplegia using a hand neuroprosthesis," *J. Hand Surg.,* **19A** (1994) 209-218.

[6] Harvey, L.A.; Batty, J.; Jones, R.; Crosbie, J. "Hand function of C6 and C7 tetraplegics 1-16 years following injury," *Spinal Cord* **39** (2001) 37-43.